CLASSIFICATION:
Open

OSLO METROPOLITAN UNIVERSITY
STORBYUNIVERSITETET

Department of Civil Engineering and Energy Technologly – Energy and Environment
Postal address: P.O.box 4 St. Olavs plass, N-0130 Oslo, Norway
Visiting address: Pilestredet 35, Oslo
Website: www.oslomet.no

MASTER'S THESIS

TITLE:	SUBMISSION DATE:
Analysis of human cough in confined spaces: a numerical study	30th June, 2021
	NO OF PAGES & APPENDICES: 74 / 5
AUTHORS: Patrick Paulsen	SUPERVISOR: Arnab Chaudhuri

DONE IN COLLABORATION WITH:	CONTACT PERSON:
Convergent Science GmbH, Austria	Suresh Kumar Nambully

ABSTRACT:

The viral transmission in human could occur via different modes like large respiratory droplets, direct contact with contaminated surfaces and airborne microdroplets or aerosol in indoor environment. During breathing, talking, singing, coughing, or sneezing an infected person exhales particles that is contagious for others. This study revisited the human cough instances in an elevator setup using advanced three-dimensional adaptive mesh refinement based computational fluid dynamics multiphase flow solver. This work presented the demonstration of AMR based 3D simulation, analysis of saliva droplet dynamics, effect of relative humidity to enlighten the uncertainties and challenges connected to airborne transmission virus in confined space.

KEYWORDS (one per line):

Computational fluid dynamics (CFD)
Adaptive mesh refinement (AMR)
Multiphase turbulent flow

PREFACE

This master thesis represents the end of a master's degree in "Energi og miljø i bygg – sivilingeniør" at Oslo Metropolitan university. The work in this thesis have been done in the spring 2021.

I will begin by saying a huge thanks to my supervisor Arnab Chaudhuri who have been available for me day and night when needed answer to all dumb questions and taken the time to explain and educate me along this process. This has been a weird semester due to Covid-19, the students have been separated, the school have been closed over half of the semester, so without your motivational attitude I would never have been done with this work. So many thanks.

The Challenge of learning a new CFD solving tool also takes a huge amount of time, on top of other things. So, I will send a big thanks to Mr. Suresh Kumar Nambully from Convergent Science GmbH for being available for questions, explanations and clarifying problems due to the process of learning Converge CFD solving tool.

At last, I would say a shout out to my fellow students. Even though we were not able to spend so much studying time together this semester, our good relationships from the time here at OsloMet have been a good motivation and safety throughout this semester.

Now my time is over here at OsloMet. Thanks for a nice experience and two good years.

ABSTRACT

The current global pandemic situation demands to gain more knowledge and understanding about viral transmission in indoor environments. Thorough knowledge of breathing, talking, coughing, singing, and sneezing of human beings in connection with infection spread is quint essential for designing mitigation measures for indoor environments.

The main objective of the study is to revisit the human cough instances in an elevator setup using advanced three-dimensional adaptive mesh refinement (AMR) based computational fluid dynamics multiphase flow solver. The present work makes use of the computationally effective AMR method to resolve unsteady complex flow physics involving heat and mass transfer in a turbulent multiphase flow. The Eulerian dispersion medium is considered as a multicomponent ideal gas mixture consisting of O2, N2 and H2O and the Lagrangian dispersed phase of human cough is considered as pure liquid water.

Simulations are performed to demonstrate the effectiveness of AMR based 3D simulations with varying AMR embedding scale. Evolution of different liquid phase size distributions has been studied by varying the number of liquid parcels. Finally, the effect of relative humidity is investigated for single cough instances. The results show about 35% evaporation for RH of 40% for 7.7 μg liquid injection for cough instance including a droplet travel distance for nearly 1.6m in the streamwise direction.

SAMMENDRAG

Den pågående globale pandemien krever at vi fordyper oss i kunnskap og forståelse knyttet til viral overførsel av smittsomme dråpepartikler i innendørs miljø. Grundig kunnskap om pusting, snakking, hoste, synge og nys av mennesker i forbindelse med infeksjonsspredning er viktig for å utforme tiltak og forebygge smitte innendørs.

Formålet med studiet er å analysere forekomsten av menneskelig hoste i en heis ved hjelp av avansert tredimensjonalt AMR basert verktøy basert på CFD for flerfase strømning. Arbeidet bruker den beregningseffektive AMR-metoden for å løse en turbulent kompleks strømningsfysikk som involverer varme -og masseoverføring i en turbulent flerfasestrøm. Eulerian-despersonsmediet betraktes som en ideell gassblanding med flere komponenter bestående av O2, N2 og H2O, og den Lagrangian-spredte fasen av menneskelig hoste betraktes som rent flytende vann.

Simuleringer utføres for å demonstrere effektiviteten av AMR-baserte 3D-simuleringer med varierende AMR- skalering. Utviklingen av forskjellige væskefasestørrelsesfordelinger har blitt studert ved å variere antall væskepakker. Til slutt blir effekten av relativ fuktighet undersøkt for hoste. Resultatene viser om lag 35% fordampning for RH på 40% for 7,7 μg væskeinjeksjon for hoste, inkludert dråpespredning i nesten 1,6 meter i strømnings retning.

CONTENT

List of tables

List of figures

1 INTRODUCTION

We are all affected in some way by the global pandemic that is going on around the world these days. About 140 million people are infected and nearly 3 million deaths in the end of April 20201 due to COVID-19. In Norway, the number is just over 100000 infected and 700 deaths. The difference between this pandemic and similar situations in the past, is the technology to cope and possibly understanding the way airborne virus transmission work. This is essential because the earth is more populated than ever, along with the fact that people all over the world can travel across land borders and continents easier and cheaper than only twenty years ago. The events of the past year and a half will possibly affect how we relate to people and situations for many years to come.

During the timeline of this pandemic, the original SARS-CoV-2 (covid), has mutated into even more contagious version, such as the Alpha (English), Beta (South-African), Gamma (Brazilian) and Delta (Indian) variant. The changes in everyday life are many and tough to bear for a lot of people. The cultural happenings like theatre, cinema, etc. are all stopped and closed. Public transport is being recommended not to use, keeping a safe distance to others and reduce the number of people to socialize with are just some of the major changes that have an impact on people on a regular basis. The use of face mask has become normal as well as washing/disinfect hands after touching anything outside where you live. All this is to make sure we do all that we can do stop and/or control the spread of the infection which is believed happen by various modes. With this in mind, it is important to understand the COVID-19 viral transmission in indoor environments.

From an evolutionary perspective the mutations from the organism in e.g., the COVID-19 virus, is normal and expected. Even if the mutated version infects easier and by that have the potential to reach more humans, it will also most likely be less dangerous for the average person. As the virus, wants to stay alive in its host for the longest period, it cannot survive on a strategy where the host has a high death ratio. Therefore, it adapts various times to coexist for the longest with the virus carrier.

1.1 Mode of spreading of the COVID-19

The viral transmission in human could occur via different modes like large respiratory droplets, direct contact with contaminated surfaces and airborne microdroplets or aerosol in indoor environment. During breathing, talking, singing, coughing, or sneezing an infected person exhales particles that is contagious for other. We summarize the various modes of viral transmission below.

Direct contact with contaminated surfaces for so to get infected trough mucous membrane in mouth, nose, or eyes is one way. Another is close contact with infected person. World Health Organization recommend not closer than one meter (WHO). Here, infection comes from droplets that contain the virus, for so to be inhaled or come in direct contact with mucous membrane in mouth, nose, or eyes. The last mode might also be the hardest to protect against. Current evidence suggest that aerosol is the hidden way of spread in indoor environments. These are tiny droplets which can stay floating in the air for a long period of time. They are too small for gravity to pull them to the ground but still as contagious. The Spanish paper El Paìs showed a model where people can play with situations to see the effect of aerosols (Zafra, 2020). This model is made by the university of Colorado and show how it is possible to predict the chance for infection due to different infection control measures. This type of model is not hundred percent accurate but can give a general understanding of how the aerosols behave

The particles that come from the human body (mouth, nose, eyes) have a range in size where the larger ones are respiratory droplets, and the smaller ones are aerosol particles. The larger ones often fall towards the ground due to gravity. While the aerosols evaporate faster than they settle so they can hover in the air for a longer period. (Greenhalgh et al., 2021b)

Till now the scientific findings are insufficient to conclude that the SARS-CoV-2 spread through airborne transmission. There is evidence supporting exactly this (Greenhalgh et al., 2021a).

1.2 OBJECTIVE OF STUDY

Understanding of breathing, talking, coughing and sneezing of human beings in connection with infection spread is quint essential for designing mitigation measures for indoor environments. Careful considerations of the local airflow, source proximity, droplet dispersion/evaporation, Air change per hour, relative humidity must be taken into account to understand the viral transmission and designing preventive measures. The main objective of the study is to revisit the human cough instances in an elevator setup using advanced three-dimensional adaptive mesh refinement (AMR) based computational fluid dynamics multiphase flow solver. This work will present relevant literature findings and will involve consideration of Eulerian multicomponent compressible continuous phase and Lagrangian approach for liquid droplets to resolve droplet dynamics and effect of relative humidity.

To present this clear and precise the thesis is organized in the following way. First section contains a literary survey of recently done CFD work. Then chapter two includes the main theory and governing equations used throughout the simulations. In Chapter three, we present the methodology and the problem setup which is the definition and calculation of input values regarding geometry, computational domain, grid control, physical and chemical phenomena that needs modeling as well as setting up boundary conditions. Chapter four presenting the results and including discussion. This is followed by the results and discussions in Chapter four. Finally, conclusions and future works are presented in Chapter five.

1.3 LITERATURE REVIEW

By studying other articles and CFD work, it is possible to get a wider and clearer overview of an already complex topic. While the usage of CFD to understand multiphase flow in terms of airborne transmission is relatively new, there have been published some articles involving this theme the last 1-2 years. We are going to have a short but relevant literature survey about recently relevant articles, for enlightenment and validation. And focus our limited time on the pre process and introduction to the new CFD simulation tool presented in this thesis.

A Eulerian-lagrangian modeling of cough droplets was done by V. D'Alessandro (D'Alessandro et al., 2021) recently. The goal was to gain new insight into the transport of fluids and particles originated from coughing, and due to covid-19. The simulation was done without any affection of wind, and some of the models used are similar in this study. The Rosin-Rammler probability density function distribution is used and a high number of particles, around 20000, which also is relevant for our simulation. Some of the interesting results according to this thesis was the particles distribution as well as the particles travel distance, which is similar to our with a mean distribution at 81.87 μm and a particle travel distance at 1.8m horizontally. We will see this closer in section 4.3

A similar case with a different angle was done by (Sen, 2021) where they used a Euler-Lagrangian approach to simulate transmission and evaporation of micrometer-seized droplet generated due to coughing by both one and several persons inside a lift. The model was simulated both with and without a roof fan for air supply and different relative humidity values were tested. Their focus is on direction of evaporation than this study, but we can draw some comparison regarding the evaporation rate they found. With a rate of 75% evaporation ratio on the case with RH 30% we can correlate with one of our simulated cases. See result section 4.4 for further information.

(Dbouk & Drikakis, 2021) is another new study we will revisit during this thesis. They investigated the respiratory droplet dynamics from a cough in a confined space. Having a single human and focus on air supply they use look at different variables due to positioning and airflows inside the elevator. The computational mesh used varies from around 285000 cells to the finest grid, 594000 cells. This is many times the amount our mesh will be, but due to the adaptive mesh refinement we still will see similar results when we revisit their results about the droplets air movement distance, which was found to be 1.7m, see results 4.4.

A numerical study done by Yo Zhou (Zhou & Ji, 2021) where the risk of infection due to the existing ventilation system as well as a relatively closed indoor environment in hospital/fever clinic looks at the transport of droplets aerosol generated by both patients and doctors, and seek ways to reduce the risk of infection. Both cough and talk and different contact distances on the inhalation rate of droplet aerosols was studied. This study uses a high amount of 40000 particles, which we will visit in one of our simulations, see section 4.3. This article takes breathing into consideration, which we do not, but it gives a wider understanding of indoor contamination.

The computational studies of a human sneeze were modelled with the help of CFD (Busco et al., 2020) to understand the sneeze dynamics. The objective is to accurately predict the spread of aerosol and droplets that may contain infectious pathogen. With a bit different approach then this thesis, they conclude with the fact that sneezing is the most violent spasmatic expiration of a mixture of moist air and saliva. This is in comparison of another article mention in this study (Dbouk & Drikakis, 2020a).

A study to understand and characterize the flow dynamic of a cough was done with coughs from human subjects by Gupta (Gupta et al., 2009) and from this they found out that a violent expiratory behaviour, such as a cough, has a cone angle of 65º, which is used in this thesis for the cough angle, shown in table 6.

An article that addresses the risk of inhaling potentially virus-containing particles indoor had some relevant information (Shao et al., 2020). Through experimentation using Schlieren imaging they combine in situ measurements and computational fluid dynamics simulations. One of the scenarios is particle spread in an elevator. And the results shows that the ventilation design is crucial for the efficiency of particle removal. Without a good ventilation strategy, it will create local hot spots with orders of magnitude higher risks along with surface contamination. Different settings are simulated such as breathe and talk. This will naturally change the number of exhaled particles. The result show that with the highest chosen ventilation (30ACH) only about 15% of the desired particles will be ventilated out. It further emerges that under selected conditions, ventilation can also contribute to dispersing particles over greater distances, which can have a negative outcome in an elevator situation as infected particles can spread out of the elevator and into the corridors etc.

Almost all of these articles are relatively newly published and use CFD as simulation tool. Some of them are directly looking at similar settings and variables as this thesis, and some are

generally relevant, but none of them are using AMR (see 3.1) as a method for grid control, which this thesis will use.

1.3.1 RECENT STUDIES INVOLVING COUGH INSTANCES

To get some more insight to previous work with a different approach that this thesis, an overview about some recently CFD studies and cases are shown below.

TABLE 1 PREVIOUSLY DONE CFD SIMULATIONS PART A

Part A

	Eulerian-Lagrangian modeling of cough droplets irrradiated by ultraviolent light in relation to sars D'Alessandro	On respiratory droplets and face masks Dbouk	Distribution of virus carrying saliva froplets during sneeze and cough (both mask Pendar	Fluid dyn. study of transmission of respiratory droplets trough a facemask filter with a cough Dbouk
T	34 °C mouth 25 C surroundings 20 itial t of carrier	34 °C 32 face skin °C °C	34 °C mouth 20 ' surroundings	34 °C mouth 20 ' surroundings
RH	50 %	50 % %		
		%		
Ventilation			0.6 m/s air cond 0.2 m/s air cond	
Duration of injection	0.12 s	0.12 s		
mean droplet				80 µm average
Distribution				
n			33 °C	
mouth area	2x10-4 m2		314 mm2	
Total mass droplets	7.7 mg		15 mg	7.7 mg
Particles size range	µm		90-540 µm	
Velocity	8.5 m/s	5 m/s	6.3-22.3 m/s	
Number parcels				1008 parcels
Elevator size				

TABLE 2 PREVIOUSLY DONE CFD SIMULATIONS PART B

Part B

	Influence of wind and relative humidity on the social distancing effectivness to prevent covid 19 Feng	Transmission and evaporation of cough droplets in an elevator: Numerical simulations of some possible scenarios Sen	Experimental and numerical study on the transport of droplet aerosols generated by occupants in a fever clinic Zhou
T	37 °C mouth	37 °C 25 °C surroundings	31 18 ventilasjon 35 cough/talk
RH	40 % 99.5 %	0 % 90 %	90 % cough 40 % inhlet air
Ventilation		0.67 m diam. Fan 0.0 ,0.25 , 0.5 m/s velocity	1.08 m/s inhlet air
Duration of injection	0.5 s	0.12s cough	2s cough
mean droplet		80 µm average	
Distribution		8	
n			
mouth area	10 mm Hydr. Mouth diam	40 x 0.8 mm2	
Total mass droplets		7.7 mg	
Particles size range	50-200 µm		
Velocity		8.5 m/s	11.2 m/s
Number parcels			40000 particles
Elevator size		1.5x1.5x2 m3	

2 THEORY

This section the method and theory are presented. This involves the governing equations of fluid flow, initial and boundary conditions, and the numerical setup for the simulations.

2.1 GOVERNING EQUATIONS

Governing equations for fluid flow are used to solve the flow-field variables. This includes the mass and energy conservation equations as well as the compressible Navier-Stokes equations. Essentially, for unsteady flow-field, we find the spatio-temporal distribution of the following variables: $\rho, P, T, \vec{V}, \Upsilon_{O_2}, \Upsilon_{N_2}, \Upsilon_{H_2O}, \varepsilon, \kappa$, where:

TABLE 3 UNKNOW VARIABLES SOLVED BY GOUVERING EQUATIONS

Unknown variable	Description
ρ	Density
P	Pressure
T	Temperature
$\vec{V}$	Velocity vector (x, y, z-plane)
Υ_{O_2}	Mass fraction oxygen
Υ_{N_2}	Mass fraction nitrogen
Υ_{H_2O}	Mass fraction water
κ	Turbulent kinetic energy
ε	Rate of dissipation of turbulent energy

The saliva droplets are solved assumed water as working fluid.

2.1.1 EULERIAN PHASE

continuum eq.

The continuum eq., which is an unsteady, three-dimensional equation for a compressible fluid is given by:

$$\frac{\partial \rho}{\partial t} + \nabla * (\rho \boldsymbol{u}) = S \tag{1}$$

Where ρ is density, t is time, u is the velocity and S is source term. S is non zero in cases with evaporation.

Navier stokes equations

The Navier stokes equations are gives by:

$$\frac{\partial \rho u_i}{\partial t} + \frac{\partial \rho u_{ij}}{\partial x_j} = -\frac{\partial P}{\partial x_i} + \frac{\partial \sigma_{ij}}{\partial x_j} + S_i \tag{2}$$

Where ρ is density, u is velocity, t is time, P is pressure, σ is viscous stress tensor and S is source term.

The viscous stress tensor is the stress at some point within a material that can be attributed to the rate at which is deforming around that given point, and is given by:

$$\sigma_{ij} = \mu\left(\frac{\partial u_i}{\partial x_j} + \frac{\partial u_j}{\partial x_i}\right) + (\mu' - \frac{2}{3}\mu)(\frac{\partial u_k}{\partial x_k}\delta_{ij}) \tag{3}$$

Where μ' is dilatational viscosity (zero), μ is viscosity, δ is' the Kronecker delta, P is pressure. The S_i can come from for example gravity.

The suffix notation σ_{ij} indicate the direction of the viscous stresses. this means that i and j specify that the stress component acts in the j-direction on a surface normal to the i-direction.

Equation of state

The equation of state is necessary to link pressure, temperature, and density. For the compressible multicomponent gas mixture, the ideal gas law is used.

$$P = \rho RT \tag{4}$$

R is ideal gas constant, T is temperature, ρ is density and P is pressure.

Energy equation

Energy equation in compressible form is

$$\rho\frac{\partial e}{\partial t} + \rho\frac{\partial u_j e}{\partial x_j} = -P\frac{\partial u_j}{\partial x_j} + \frac{\partial}{\partial x_j}\left(\frac{K}{c_v}\frac{\partial e}{\partial x_j}\right) + \sigma_{ij}\frac{\partial u_i}{\partial x_j} + \frac{\partial}{\partial x_j}\left[\left(\sum_m h_m \rho D - \sum_m e_m \gamma \frac{K}{c_p}\right)\frac{\partial \Upsilon_m}{\partial x_j}\right] \tag{5}$$

Υ_m is mass fraction of species *m*, D is the mass diffusion coefficient, P is pressure, *e* is specific internal energy, K is the conductivity, h_m is the species-specific enthalpy, c_p and c_v is respectively specific heats at constant pressure and volume, and γ is the specific heat ratio.

For turbulence modelling conductivity is replaced with turbulence conductivity:

$$K_t = K + c_p \frac{\mu_t}{Pr_t} \tag{6}$$

Where Prandtl number is

$$Pr_t = \frac{c_p \mu_t}{k_t} \tag{7}$$

μ_t is the turbulent viscosity and k_t are turbulent conductivity.

Species transport equation

The compressible form of the species conservation equation is given by:

$$\frac{\partial \rho_m}{\partial t} + \frac{\partial \rho_m u_j}{\partial x_j} = \frac{\partial}{\partial x_j}\left(\rho D_t \frac{\partial \Upsilon_m}{\partial x_j}\right) + S_m \tag{8}$$

ρ_m is species density, Υ_m is mass fraction of species m, D_t is the mass diffusion coefficient and S_m is source term.

For a turbulence model such as this, the molecular mass diffusant coefficient is calculated by:

$$D_t = \frac{v_t}{Sc_t} \tag{9}$$

Where Sc_t is the turbulence Schmidt number, v_t is turbulent kinematic viscosity

RANS, Reynolds-Averaged Navier-Stokes

In turbulent flow-field we solve Reynolds-Averaged Navier-Stokes equations (RANS), which takes the governing equations as described in previously section and decompose them into fluctuating and time-averaged (sum of the mean) quantities, as shown under by example of velocity:

$$u(x,y,z) = \overline{u(x,y,z)} + u'(x,y,z) \tag{10}$$

$$u_i = \bar{u}_i + u_i' \tag{11}$$

Where $\bar{u}$ are the ensemble mean velocity, u is the instantaneous velocity and u' are fluctuations velocity or deviations from the expected value.

To derive the RANS transport equation and averaging, substitute the equation above into Navier-Stokes eq. Then the compressible RANS equation for mass and momentum transport becomes (the continuity equation becomes):

$$\frac{\partial \bar{\rho}}{\partial t} + \frac{\partial \bar{\rho}\tilde{u}_j}{\partial x_j} = 0 \tag{12}$$

And

$$\frac{\partial \bar{\rho}\widetilde{u_\iota}}{\partial t} + \frac{\partial \bar{\rho}\widetilde{u_\iota u_J}}{\partial x_j} = -\frac{\partial \bar{P}}{\partial x_i} + \frac{\partial}{\partial x_j}\left[\mu\left(\frac{\partial \widetilde{u_\iota}}{\partial x_j} + \frac{\partial \widetilde{u_j}}{\partial x_i}\right) - \frac{2}{3}\mu\frac{\partial \widetilde{u_k}}{\partial x_k}\delta_{ij}\right] + \frac{\partial}{\partial x_j}(-\bar{\rho}\widetilde{u_\iota' u_J'}) \tag{13}$$

Where the Favre average, ~, is defined for velocity as:

$$\widetilde{u_i} \equiv \frac{\overline{\rho u_i}}{\overline{\rho}} \tag{14}$$

When ensemble averaging of the equations it introduces an additional term, the Reynolds Stresses, that represents the effects of turbulence. The purpose for this is to clarify if the flow is laminar, turbulent, or in between. The Reynolds stress is given by:

$$\tau_{ij} = -\bar{\rho}\widetilde{u_{ij}'} \tag{15}$$

To solve the mass fraction of all the species in the domain, the following species transport equations are solved.

$$\Upsilon_m = \frac{M_m}{M_{tot}} = \frac{\rho_m}{\rho_{tot}} \tag{16}$$

Where M_m is the mass of species m in the cell, M_{tot} is the total mass in the cell, ρ_m and ρ_{tot} is density of species and density of the cell.

2.2 TURBULENCE MODELS

For the CFD analysis to be as accurate as possible it is important to choose a fitting turbulence model to solve the RANS equations. For a good prediction of the mixed air/water flow from coughing the model needs to be able to explain the mixed flow behaviour well.

The two-equation relizable k-ε model is used. Where the turbulent kinetic flow, k and the dissipation, ε-equation are solved for the turbulent flow. k determinate the energy in turbulence and e determinate the rate of dissipation of the turbulence kinetic energy. The advantage of the realizable version of the k-ε model is that we avoid getting negative values for the turbulent kinetic energy, which can happen if the mean strain rate is high for example. Also, it is reliable for free-share flows, with relatively small pressure gradients.

eq. k-ε

$$\frac{\partial \rho k}{\partial t} + \frac{\partial (\rho u_i k)}{\partial x_i} = \tau_{ij} \frac{\partial u_i}{\partial x_j} + \frac{\partial}{\partial x_j} \frac{\mu + \mu_t}{Pr_k} \frac{\partial k}{\partial x_j} - \rho \varepsilon + \frac{C_s}{1.5} S_s \tag{17}$$

$$\frac{\partial \rho \varepsilon}{\partial t} + \frac{\partial (\rho u_i \varepsilon)}{\partial x_i} = \frac{\partial}{\partial x_j} \left[\left(\mu + \frac{\mu_t}{\sigma_\varepsilon} \right) \frac{\partial \varepsilon}{\partial x_j} \right] + C_1 \rho \varepsilon S - C_2 \rho \frac{\varepsilon^2}{k + \sqrt{v\varepsilon}} + C_{\varepsilon 3} \rho \varepsilon \frac{\partial u_i}{\partial x_i} + S_\varepsilon \tag{18}$$

The relizable k-ε model contains a new transport equation for the turbulent dissipation rate ε. Instead of C_μ expressed as a constant as in the standard model, here it is expressed as a function of mean flow and turbulence properties, this makes this model suitable for our problem.

2.2.1 LAGRANGIAN PHASE

The discrete phase that refers to the process of dispersion of saliva droplets throughout the computational domain is solved using a Lagrangian approach

Equation of motion

a drop's velocity, v_i , is obtained from its equation of motion:

$$\rho_l V_d \frac{dv_i}{dt} = F_{d,i} \tag{19}$$

Where $F_{d,i}$ is the sum of the drag force, $F_{drag,i}$, and the gravity body force, $F_{g,i}$, as shown below:

$$F_{d,i} = F_{drag,i} + F_{g,i} = C_D A_f \frac{\rho_g |U_i|}{2} U_i + \rho_l V_d g_i \tag{20}$$

Where A_f is the drop's frontal area, C_D is the drag coefficient, ρ_g is the gas density, U_i is the drop-gas relative velocity, ρ_l is liquid density and V_d is the drop volume.

This can be rewritten as:

$$\frac{dv_i}{dt} = \frac{3}{8}\frac{\rho_g}{\rho_l} C_D \frac{|U_i|}{r} U_i + g_i \tag{21}$$

This is used to calculate drop velocities at any given time-step.

Where the drag coefficient is:

$$C_D = C_{C,sphere}(1 + 2.632y) \tag{22}$$

y is representing the drop distortion. For example, if the spherical droplet moves through a gas, the shape will distort significantly at a high Weber number (science, 2021).

Evaporation

Once the (multiphase) liquid spray is injected into the computational domain, the Frossling correlation is used to determinate the time rate of change of droplet size so that the liquid from the saliva can be converted into gaseous vapor:

$$\frac{dr_0}{dt} = -\frac{\alpha_{spray}\rho_g D}{2\rho_l r_0} B_d Sh_d \tag{23}$$

Where α_{spray} is the specified scaling factor for the mass transfer coefficient, D is the mass diffusivity of liquid vapor in air and B_d is defined as:

$$B_d = \frac{\Upsilon_1^* - \Upsilon_1}{1 - \Upsilon_1^*} \tag{24}$$

Υ_1^* is the mass fraction at the drop's surface and Υ_1 is the vapor mass fraction. The Sherwood number, Sh_d, is given by:

$$Sh_d = (2.0 + 0.6Re_d^{\frac{1}{2}}Sc^{\frac{1}{3}})\frac{\ln(1+B_d)}{B_d} \tag{25}$$

Where

$$Re_d = \frac{\rho_{gas}|U_i|d}{\mu_{air}} \tag{26}$$

Here, d is the drop diameter and μ_{air} is the air viscosity at a temperature $\hat{T}$ which is given by:

$$\hat{T} = \frac{T_{gas} + 2T_d}{3} \tag{27}$$

In this section, we have presented the basic governing equations related to the Eulerian and Lagrangian phase. Apart from the above-mentioned governing equations, the droplet collision, droplet turbulent dispersion, droplet-wall interactions are also considered, and the corresponding equations are not presented here. A list of all relevant models and additional auxiliary models used for the simulations are provided in the following chapter.

3 METHODOLOGY

Computational fluid dynamics is the analysis of systems involving fluid flow, heat transfer and associated phenomena, such as chemical reactions done by computer-based simulation. (Malalasekera, 2007). In addition, CFD is evolving to be a vital component in the form of creating industrial products and processes. The programming concept is based around numerical algorithms that are able to tackle complex fluid flow problems. In order to provide this solution commercially their the CFD packages includes sophisticated user interfaces for input and setup parameters as well as results analysis. The buildup is universal and are as follow:

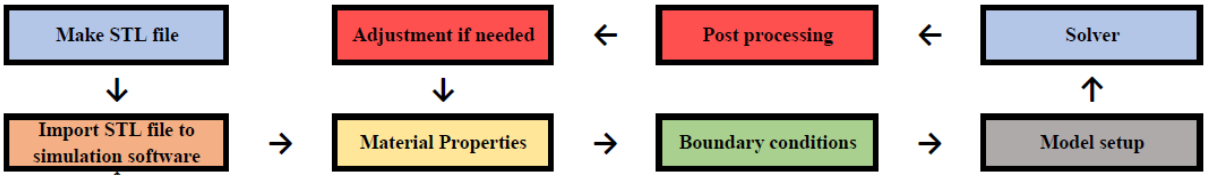

FIGURE 1 PROCESS OF CFD SIMULATION

Any CFD tool contains three main components namely pre-processor, solver and post-processor. These are defined as follows:

Pre-processor

Before simulating a CFD problem, various input values must be defined. This includes the computational domain, which is the geometry, grid control to divide the domain into mesh/grid or control volumes, choose chemical and physical phenomena that user needs modelled, define the fluid properties and specification of useful boundary conditions.

The accuracy of a simulation is governed by the number of cells in the grid. Optimal grids are in most cases non-uniform, that means its dynamically made. Finer in areas where large variations occur from point to point and coarser in regions with relatively little change. More than half of the time spend on CFD projects is normally devoted to the definition of the domain geometry and grid generation. Continuously updated pre-processors give users access to libraries of material properties for fluids and a facility to invoke special physics and chemical process models.

Solver

The most known and used CFD codes the finite volume method is central. The numerical algorithm consists of integration of the governing equations of fluid over all the finite control volumes of the domain. Then discretization, which is to convert the resulting integral equations into a system of algebraic equations and solution of the algebraic equations by an iterative method.

Post-processor

The results given by the solver step when presented, most software include additional versatile data visualization tools. This can be geometry and grid display, surface plots in both 2D and 3D, particle tracking and vector and scalar plots. Along with other tools. This gives an extra depth in terms of communicate results and analysis to non-specialist personnel (Versteeg & Malalasekera, 2007).

3.1 GRID CONTROL

In terms of generating a mesh it is important to define the position in the geometry were expected to have the greatest change of variable. This can be any flow variable such as velocity, pressure etc. depending on the problem concerned. The higher amount of cell count results in need of a more powerful computer power which again results in longer running time. This can vary from hours till days. In this work, we have considered multicomponent Eulerian gas phase (involving O2, N2 and H2O) and water (H2O) as Lagrangian phase representing the saliva droplets. Adaptive mesh refinement is chosen for generating mesh points in the computational domain.

AMR

Adaptive Mesh Refinement is a neat function that automatically refine the grid based on fluctuation and moving conditions, e.g. velocity or temperature. This feature can be used to obtain a finer grid in regions of interest allowing complex phenomena, in this case, cough, without unnecessarily slowing the simulation with a globally refined grid.

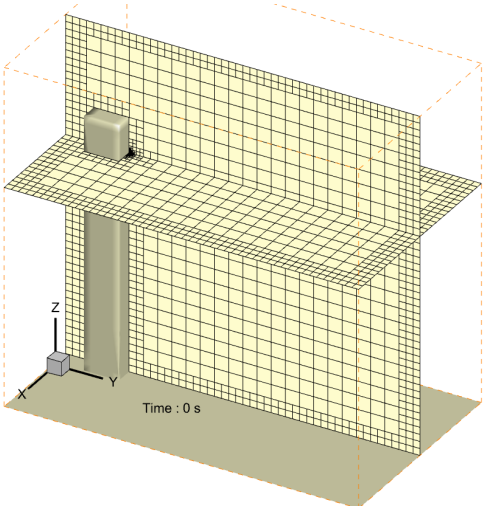

FIGURE 2 BASE OF SIMULATION. FIXED EMBEDDING MOUTH AND WALLS

We separate two different types of AMR: Sub grid scale and value based. AMR type and criteria should be chosen such that embedding (higher grid resolution) is added where the flow field is

most under-resolved, where the sub-grid field is the largest, or where a variable satisfies the embed criteria (science, 2021) see figure 2 and figure 3.

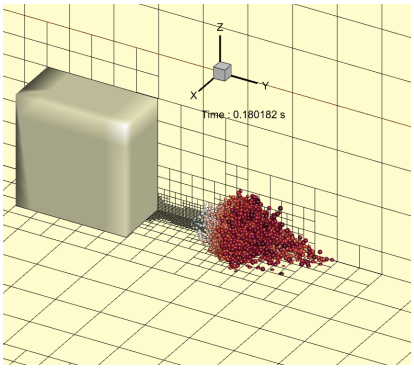

FIGURE 3 AMR EMBED SCALE OF 5

Our simulations have a fixed embedding around the mouth and wall area. This is locations in the domain where a finer resolution is critical. These settings have a scale of 5 and embed layers at 10, see figure 44 for more info. Our AMR embed scale is 5, which means how many times the cells are divided. See figure below.

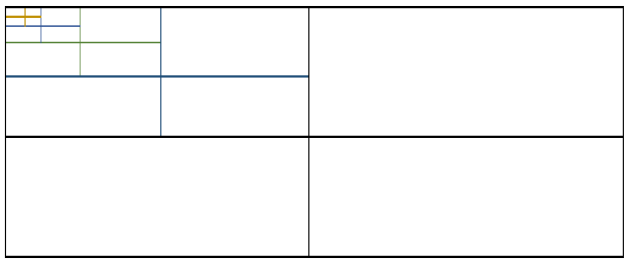

FIGURE 4 EMBED SCALE OF 5. USED IN SIMULATIONS

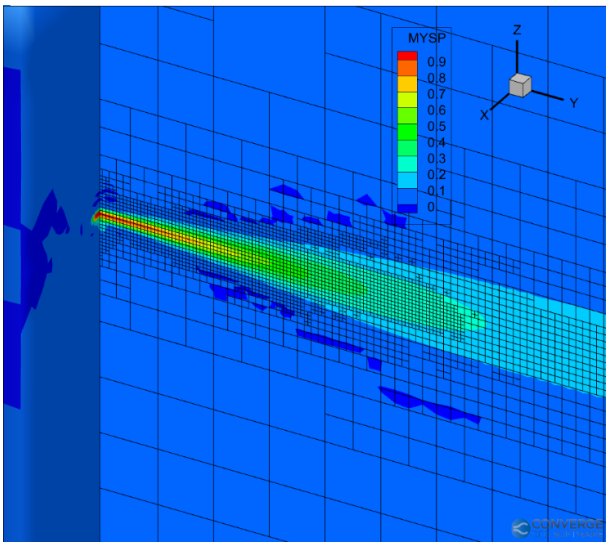

FIGURE 5 USING PASSIVE SCALAR TO SHOW GRID AROUND MOUTH

Figure 5 shows an illustration of how the grid dynamically adjust after a passive scalar in this situation. To get around the work of AMR, one simulation is done with embed scale of 2, which is shown in the figure 7. See section 4.2 for results.

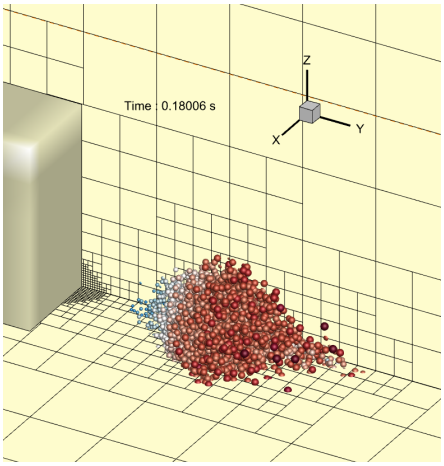

FIGURE 6 AMR EMBED SCALE OF 2

Figure 6 and figure 7 show respectively the in-work situation for the AMR with 2 as input setting and a cell in the mesh with the same input

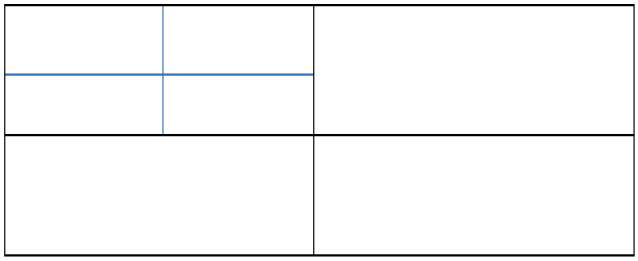

FIGURE 7 EMBEDED SCALE OF 2

FVM

Finite Volume Method used to solve the governing equations. This is an attractive method because it is highly generalizable for both non-trivial meshes and complex numerical scheme, e.g., the ones resulting from embedding.

The solver uses the finite volume method (FVM) as a solving tool. This refers to the small volume surrounding every node point on a mesh. This is done by integrating the governing equations inside a control volume, then use the resulting equations in a system of equations for then to solve them using the iterative method. Depending on the problem there are different solvers available.

PISO algorithm

The Pressure Implicit with Splitting of Operator method is an algorithm implemented in the software to start with a predictor step where the momentum equation is solved. This works as when the predictor is done, a pressure equation is derived and solved, which again lead to correction which is applied to the momentum equation. This can be repeated as many times as necessary to achieve the desired accuracy.

3.2 CONVERGE CFD SOLVING TOOL

The following models are used to simulate the human cough instances in an confined elevator setup.

TABLE 4 OVERVIEW OF USED MODELS

Gas phase models:	
Solver	Navier-Stokes solver
Navier-Stokes solver scheme	PISO
Pressure-velocity coupling	Rhie-Chow scheme
Turbulence model	RANS realizable $k-\varepsilon$
Droplet models:	
Evaporation model	Frossling model
Collision model	O'Rourke collision
Film splash model	O'Rourke
Injection model	Kelvin-Helmholtz and Rayleigh-Taylor
Particle/parcel size distribution of the liquid phase	Rosin-Rammler
Wall heat transfer model	O'Rourke and Amsden

3.3 PROBLEM SETUP

In this section, we will walk through the critical considerations for the considered test cases. At first, we present a summarize table of our simulated cases for so to have a more detailed presentation of the definition of input values. To fulfil the objective of the study we first demonstrate the AMR based 3D simulations with varying AMR embedding scale. Next, simulations are performed with varying number of droplets. Finally, the effect of relative humidity is studied for single cough instances. Table 6 include a summary of the boundary conditions.

TABLE 5 OVERVIEW OF SIMULATION CASES

Case	Relative Humidity	AMR scale	Particles/parcels	Coughs
1	-	5	20000	One
2	-	2	20000	One
3	-	5	10000	One
4	-	5	40000	One
5	40	5	20000	One
6	80	5	20000	One

3.3.1 *BOUNDARY* CONDITIONS

TABLE 6 OVERVIEW OF INPUT DATA

Elevator measurements:		
L x W x H	1.5 x 2.5 x 2.4	m
Volum	9	m3
RH average Oslo	40/60/80	%
Elevator measurements:		
L x W x H	1.5 x 2.5 x 2.4	m
Volum	9	m3
RH average Oslo	40/60/80	%
Ventilation:		
ACH and m/s	39 and 0.195m/s	
Body surface Area	1.9	m2
Cough:		
Total mass	7.7	mg
Number parcels	20000	
Velocity	8.5	m/s
Temperatur parcels	35	℃
Angle of spread	65	°
Duration exhale	0.12	s
smd	73.418	
Average size particles	80	µm
Ventilation:		
ACH and m/s	39 and 0.195m/s	
Body surface Area	1.9	m2
Cough:		
Total mass	7.7	mg
Number parcels	20000	
Velocity	8.5	m/s
Temperatur parcels	35	℃
Angle of spread	65	°
Duration exhale	0.12	s
smd	73.418	
Average size particles	80	µm

We consider an elevator as a confined space, see figure 8, together with a standing human being to simulate human cough instances with varying conditions. The different conditions are split into cases which is detailed in table 5.

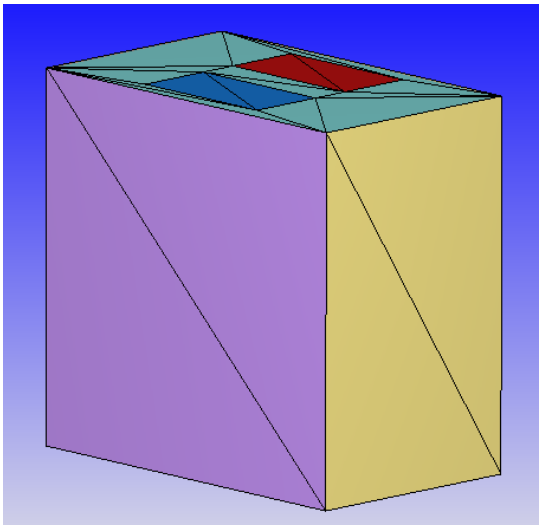

FIGURE 8 ELEVATOR CHOOSEN AS CONFINED SPACE

An elevator with dimensions (1.5 x 2.4 x 2.5) m is considered having a volume of $9m^3$, figure 9. This is the measures of an elevator at OsloMet University which is used daily. Air supply and Exhaust are two rectangles in the center of the elevator ceiling. Both inlet -and outlet area are $0.5m^2$ (1x0.5m).

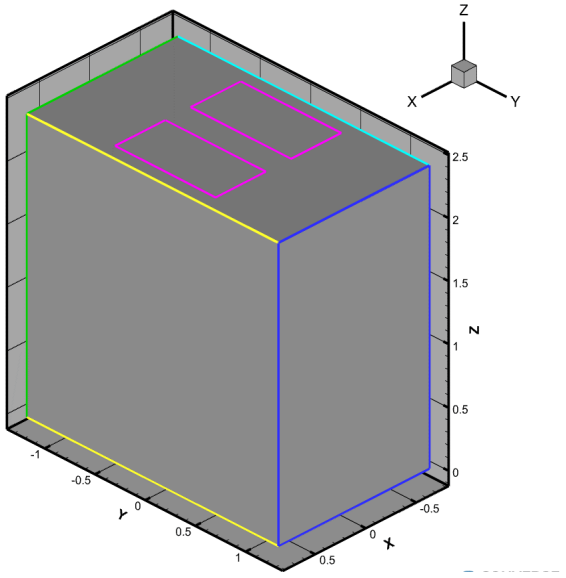

FIGURE 9 GEOMETRY ELEVATOR WITH MEASUREMENTS

Person standing in the elevator, represented as a long rectangular box which corresponds to real human dimension. This human is 1.80m tall and 1.55m to the center of the mouth. The mouth is shaped like a rectangular and have the dimensions showed in figure 10.

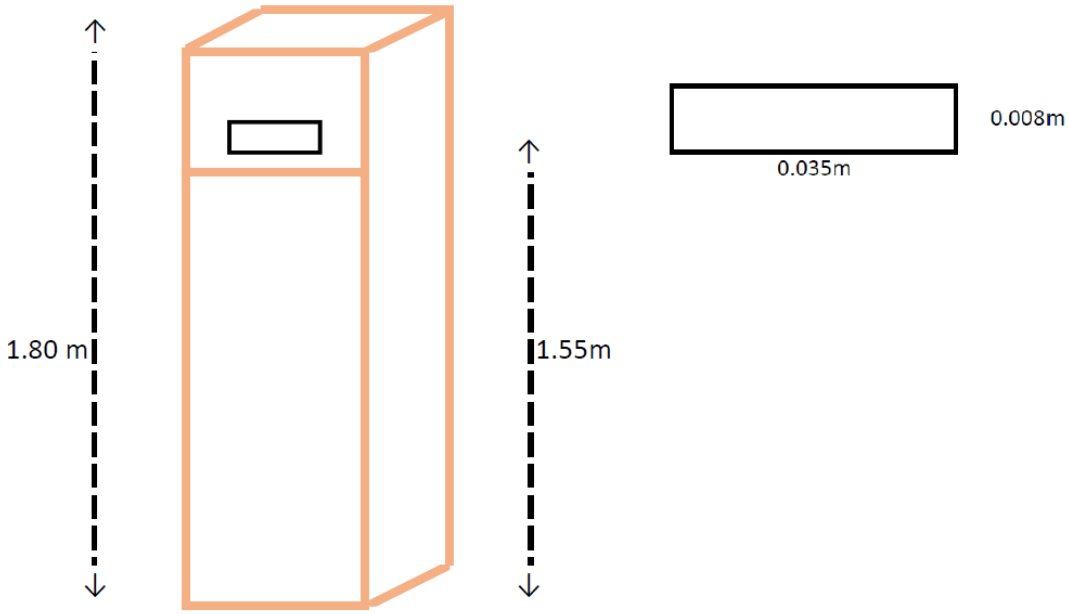

FIGURE 10 HUMAN RECTANGLE AND MOUTH WITH DIMENTIONS

Position for the human in the lift is in the back, 0.2m from the back wall and centred in the width. At the red square in the figure below.

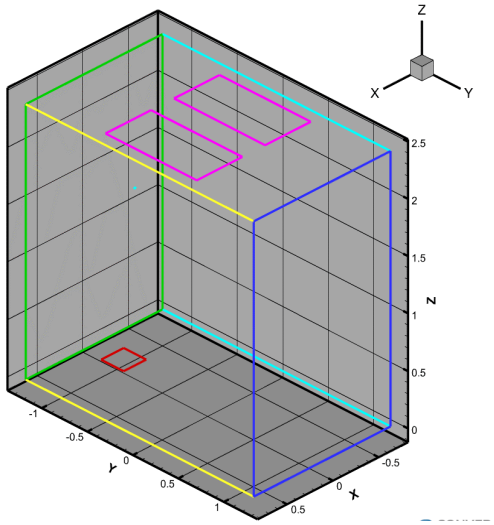

FIGURE 11 HUMAN POSITION INSIDE ELEVATOR

The cough consists of liquid water and gas mixture ($O_2 + N_2$) and are ejected from the mouth trough a nozzle as shown in figure 12.

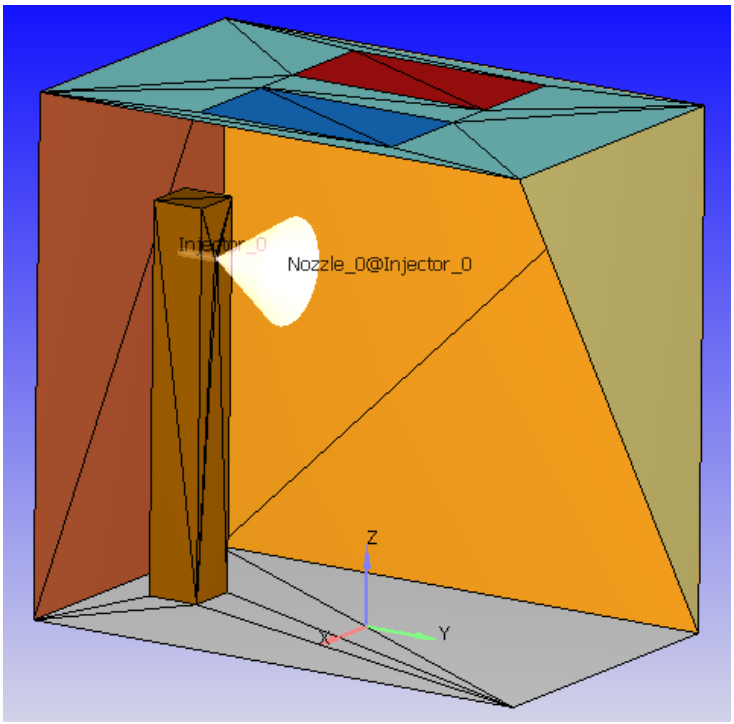

FIGURE 12 GEOMETRY INSIDE ELEVATOR

Thermal condition and duration of the cough is set to 35 ºC and 0.12s. Which is the approximation of cough exhale (Dbouk & Drikakis, 2020a). Velocity is 8.5 m/s in the streamwise direction, both from the carrier fluid and the injected parcels. The initial total mass of the saliva droplets is 7.7mg (Zhu et al., 2006) and the initial number of parcels is 20000. The particle inlet spread is set to have an angle of 65º (Gupta et al., 2009) and the water in the saliva have a density of 1000 kg/m^3 (Cengel & Ghajar, 2015).

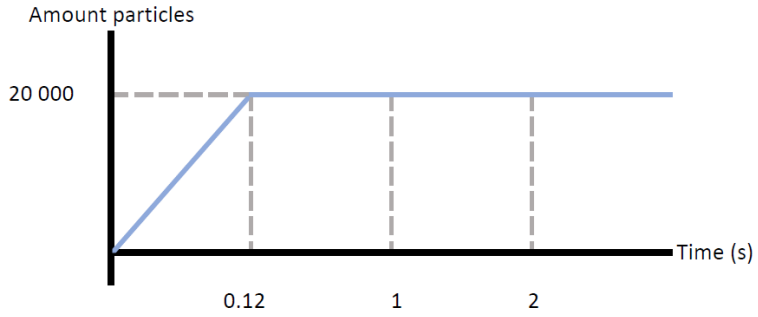

FIGURE 13 EJECTION RATE AT MOUTH FOR 20000 COUGH PARCELS

The cough cycles are shown below. The duration of each cough is set to be 0.12s. In figure 13 we can see the injection rate for the cough.

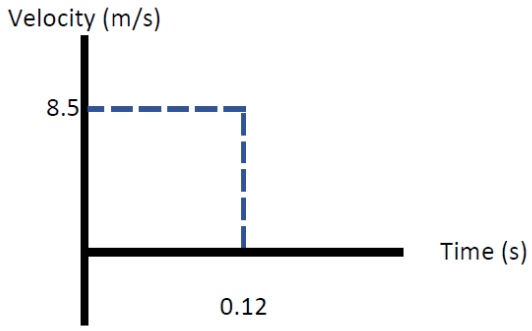

FIGURE 14 COUGH CYCLE FOR ONE COUGH

Near Wall Treatment

The near wall treatment are the conditions for the flow when it is interacting with solid surfaces. Near-wall treatment is activated for turbulence models. This grid is required to resolve the viscous sublayer may be prohibitively expensive. In these cases we use one of the wall treatments available in order to model the under-resolved viscous sublayer. The model make use of the law-of-wall assumption for velocity in the log-law region of a turbulent boundary layer. This wall function assumes that the cell adjacent to a wall lies in the log-law region(science, 2021). See section 4.1 for specified wall treatment information and validation.

Distribution

The cough droplets have a size distribution defined by Rosin-Rammler cumulative probability function. The initial size was assumed to have a mean droplet of 80μm and n = 8 (Dbouk & Drikakis, 2020b)

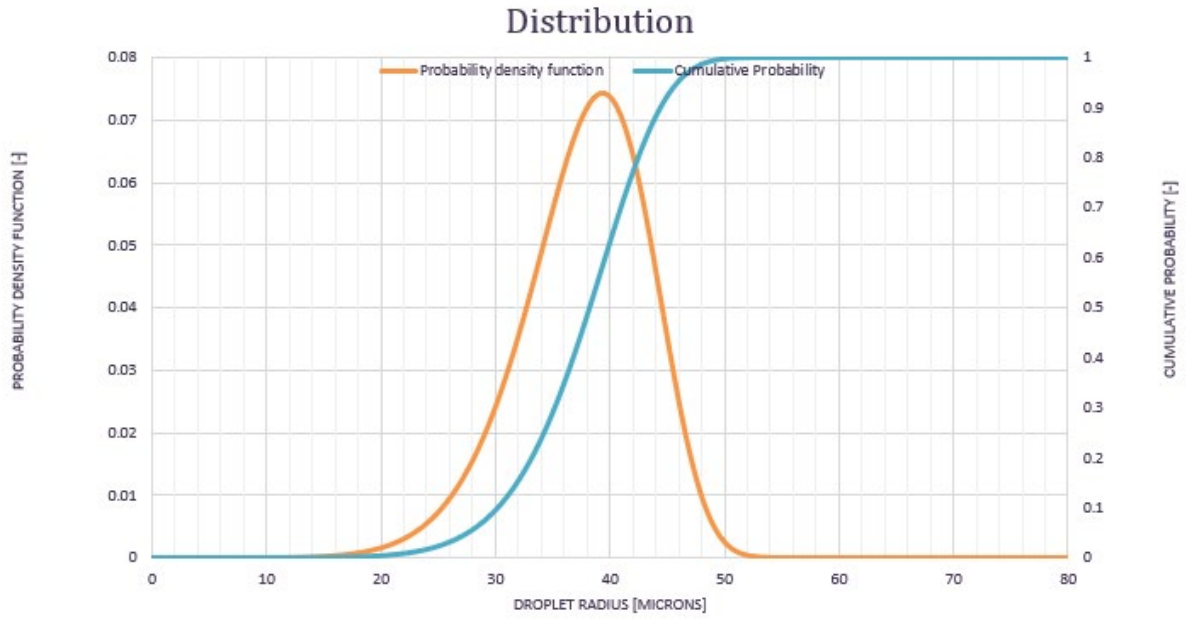

FIGURE 15 INITIAL SIZE DISTRIBUTION

The Rosin-Rammler distribution is calculated with 100 bins and are given by:

$$\tilde{R}(r) = 1 - \exp[-\zeta^q] \qquad 0<\zeta<\zeta_{max} \tag{28}$$

Where

$$\zeta = \frac{r}{\bar{r}} \tag{29}$$

$$\zeta_{max} = \ln(1000)^{\frac{1}{q}} \tag{30}$$

Here q is an empirical constant and

$$\bar{r} = \Gamma(1 - q^{-1}) r_{32} \tag{31}$$

Where Γ is the gamma function and r_{32} is the Sauter mean radius. Once a value of ζ is chosen, the injected droplets radius is determined from

$$r = \bar{r}\zeta = \Gamma(1 - q^{-1}) r_{32}\zeta \tag{32}$$

TABLE 7 SAUTER MEAN DIAMETER CALCULATED

	A	B
1	q_rr	8
2	d_bar	80
3	r_bar	40
4		
5	smd	73.41791119

	A	B
1	q_rr	8
2	d_bar	80
3	r_bar	=B2/2
4		
5	smd	=2*B3/(EKSP(GAMMALN(1-1/B1)))

Sauter mean diameter is calculated from mean diameter of the distribution (see table 7) and is the required input parameter to set the droplet distribution. The distribution curve based on the smd is shown in figure 15.

Conditions at mouth boundary

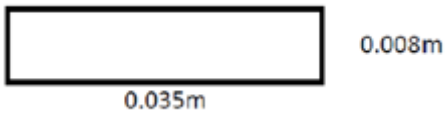

FIGURE 16 MOUTH WITH MEASUREMENTS

The mouth is set to have a rectangular shape with a length of 3.5cm and a height of 0.8cm, figure 16. The ejected parcels have a cone angle of 65º when the person coughs. The turbulence intensity is set to be 2%. The turbulente length scale is 7% of the hydraulic diameter, which is given in equation (33).

$$D_h = \frac{4ab}{2(a+b)} \tag{33}$$

Mass fraction

To find the mass fraction of the inlet air in the elevation based on relative humidity and temperature, the following steps was done:

$$P_s(T) = 0.61121\exp[\left(18.678 - \frac{T}{234.5}\right)\left(\frac{T}{257.14+T}\right)] \tag{34}$$

By using the Buck equation (Vömel, 2016) for saturated vapor pressure, based on our supply temperature, we find our P_s .

Next, we break down Air and water to find mass fractions of O_2, N_2 & H_2O based on pressure and relative humidity.

$$\omega_i = \frac{\Upsilon_i M_i}{\sum_i \Upsilon_i M_i} \tag{35}$$

Where Υ_i is mole fractions and M_i are molas masses. A detailed calculation under attachment, table 8.

air supply and exhaust

The ventilation strategy is set to be a $0.5m^2$ fan in the ceiling for supply, and the same for exhaust. As figure 17 shows.

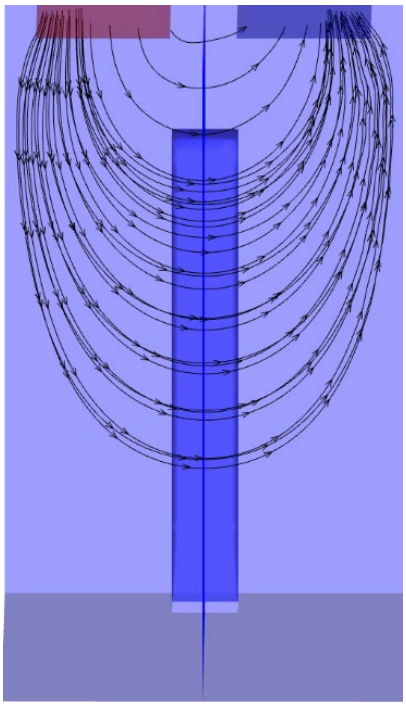

FIGURE 17 SUPPLY AIR AND EXHAUST WITH STREAMLINES

Ventilation is set to be 39ACH with respective relative humidity and temperature.

Steady state

Before injecting cough droplets, initial steady state simulations are performed to get the established airflow according to the desired ACH. This is to get the gas mixture in the confined space well mixed when doing the cough simulations. This will save computational as well as simulation time for the main case setup.

4 RESULTS & DISCUSSIONS

In this section we will present and discuss out results and validation. The cases are presented in order of table 5.

4.1 STEADY STATE INITIAL CASE

Here we present the initial steady state simulations. Those are performed to establish the multicomponent gas flow in the computational domain based on the respective ACH and RH at the air supply boundary. As mentioned before, the cough instances are simulated considering these steady state solutions as the initial conditions for unsteady liquid phase injection.

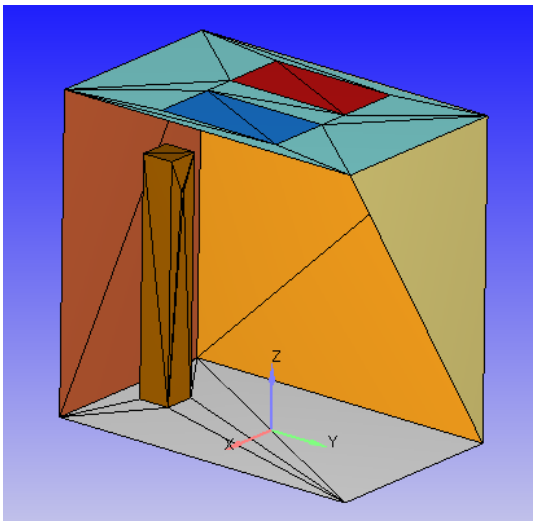

FIGURE 18 ELEVATOR WITH VENTILATION AREAS IN CEILING

Figure 18 illustrates the geometry of the steady state calculation. In this case the human will be passive.

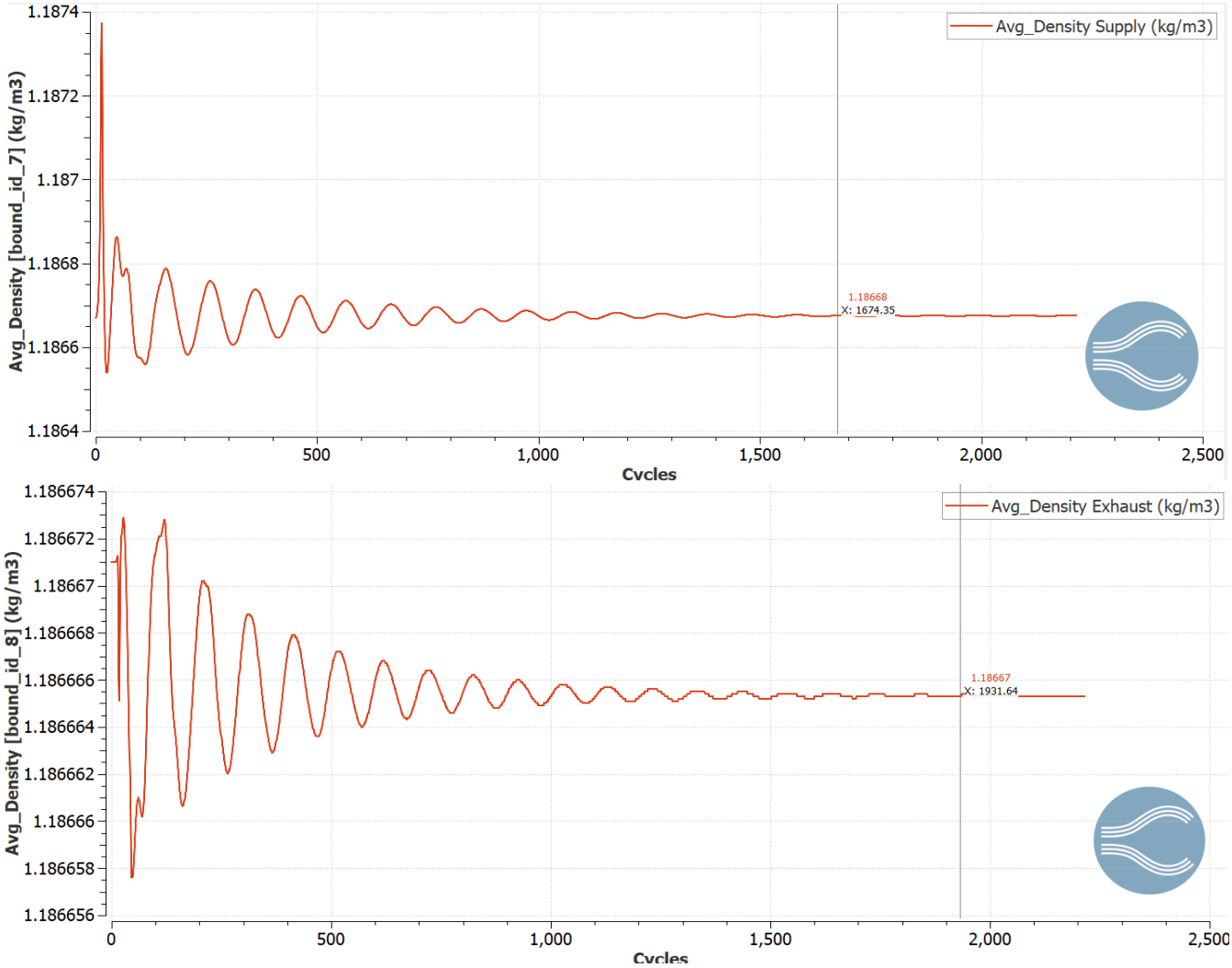

FIGURE 19 DENSITY OF AIR THAT CONVERGES

Figure 19 show convergence of density in the supply and exhaust in the steady state simulation.

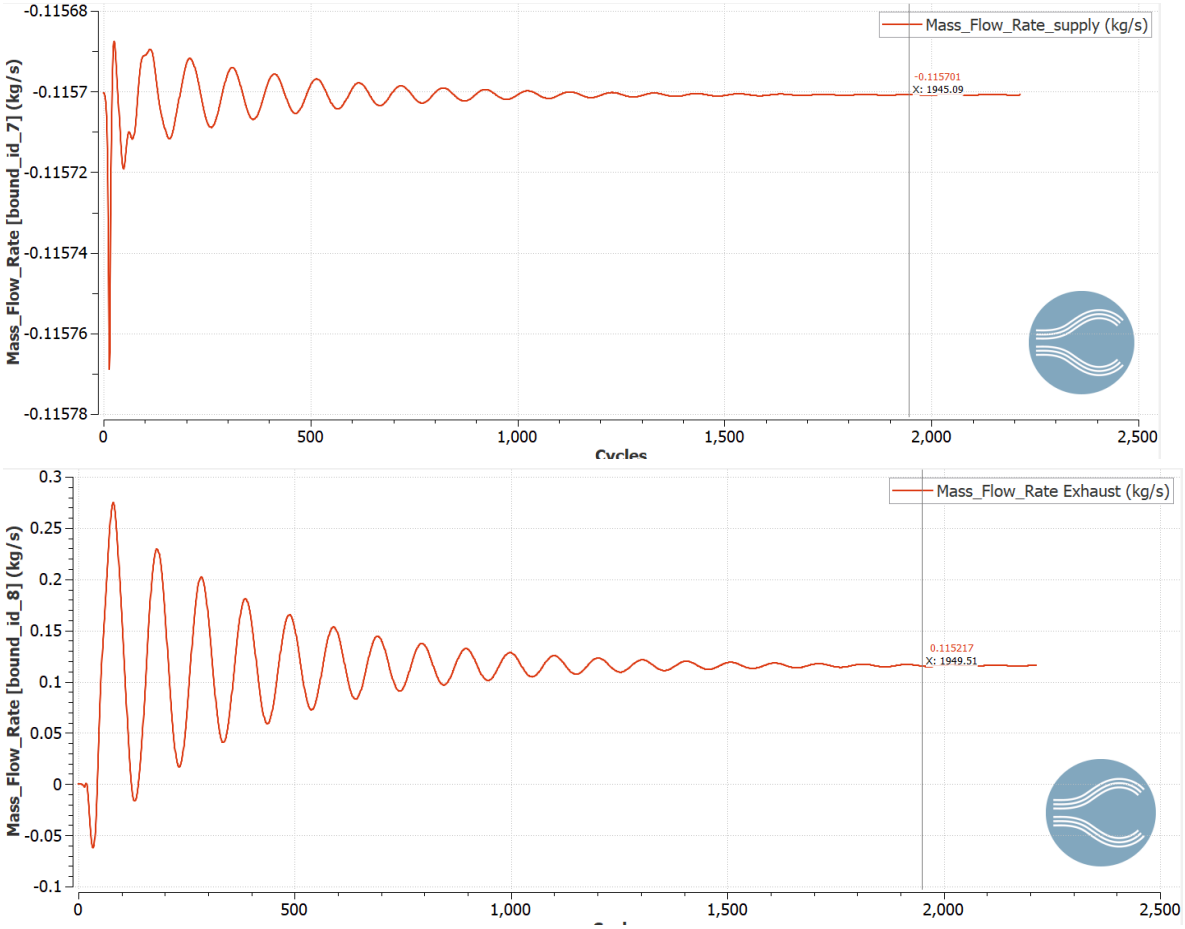

FIGURE 20 MASS FLOW RATE OF AIR THAT CONVERGES

In figure 20 we can see the mass flow rate converge to a steady flow. The mass flow rate is 0.115 kg/s at the exhaust area after our simulation stops. It is clear from figure 19 and figure 20 that we reach a steady state after our simulation stops at 2200 cycles.

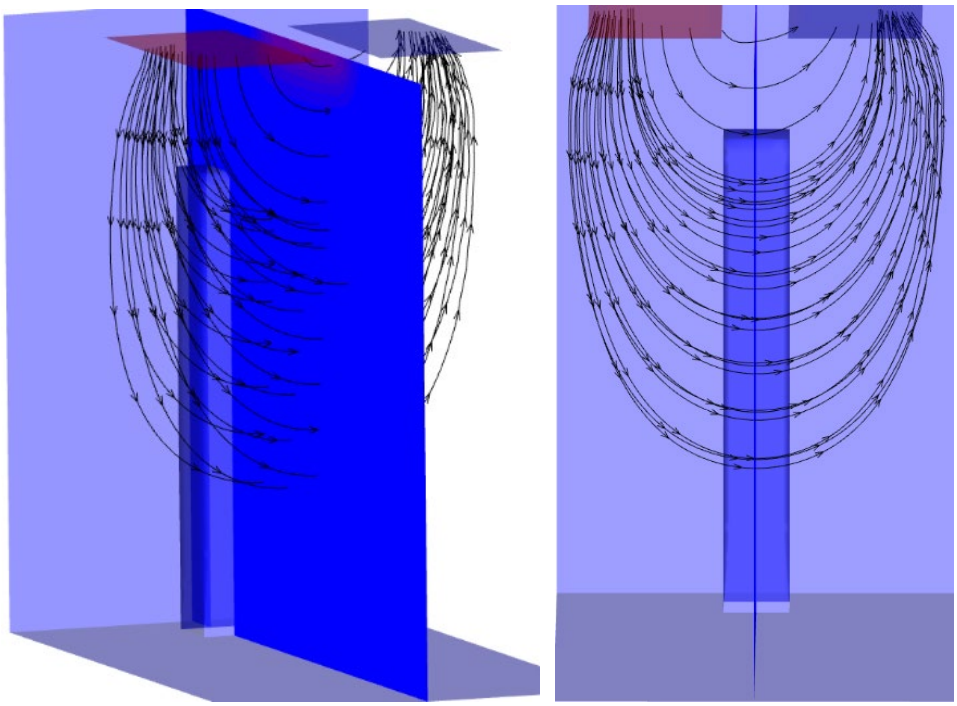

FIGURE 21 STREAMLINES AIR SUPPLY AND EXHAUST IN X-Y-Z-PLANE AND FROM THE FRONT

As the figure above shows, the air supply and exhaust have a steady flow. This steady airflow result is used as initial conditions for all the cough simulations.

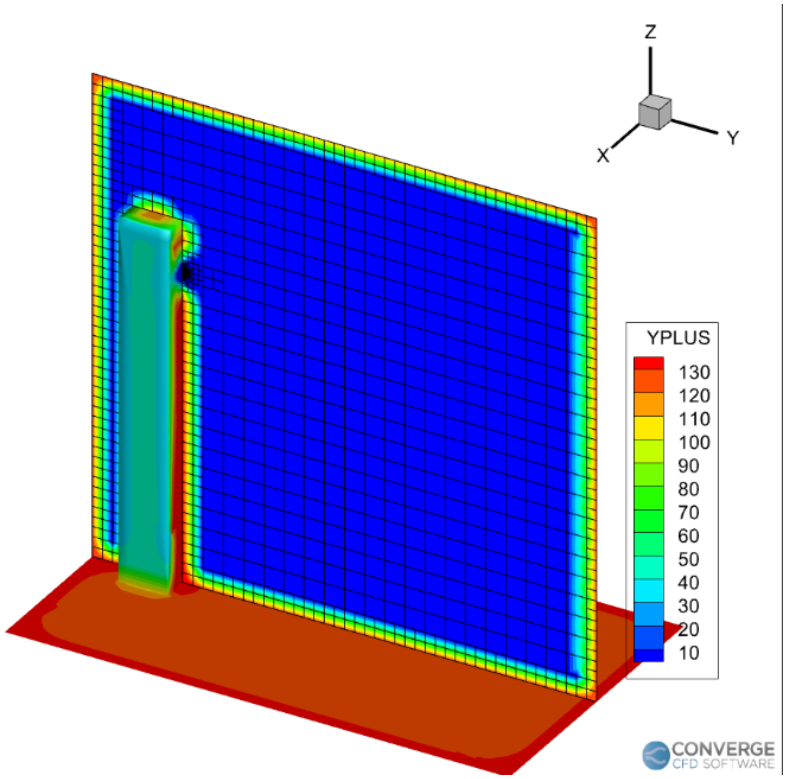

FIGURE 22 NEAR WALL TURBULENCE

Figure 22 shows that the near wall grid resolution is associated with a wall y+ value nearly in the range of 130. This falls in the log-layer region of the turbulent boundary profile (see figure 23). Since the ACH is not varied in the considered cases, the near wall fixed mesh refinement is sufficient for the near wall treatment for the two equations turbulence model used in the simulations.

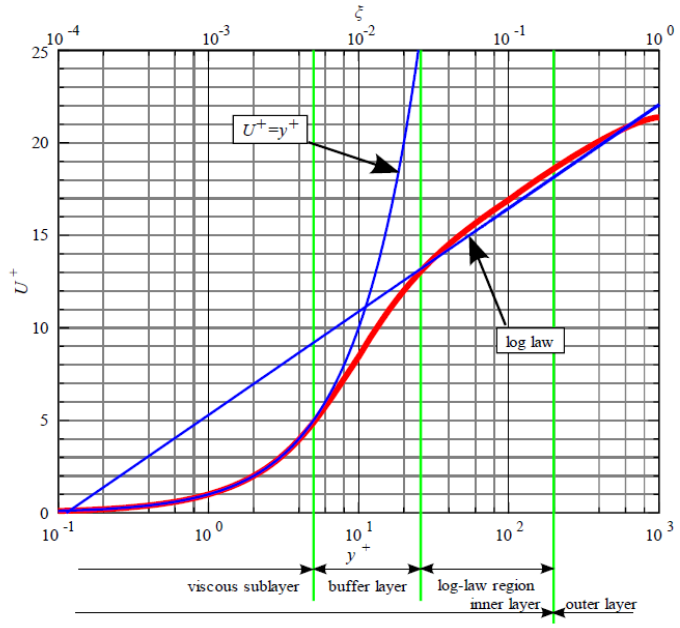

FIGURE 23 VELOCITY DISTRIBUTION NEAR A SOLID WALL (*LAW OF THE WALL*)

4.2 ADAPTIVE MESH REFINEMENT CASE 1 & 2

The effect of AMR in two identical cases with only change in AMR setting. As mentioned in Grid control section 3.1 the embed scalars are 5 and 2 in this comparison. To clarify, the use of a low grid resolution is only to show the contrast of two different settings. All other simulations tests use 5 as embed scale.

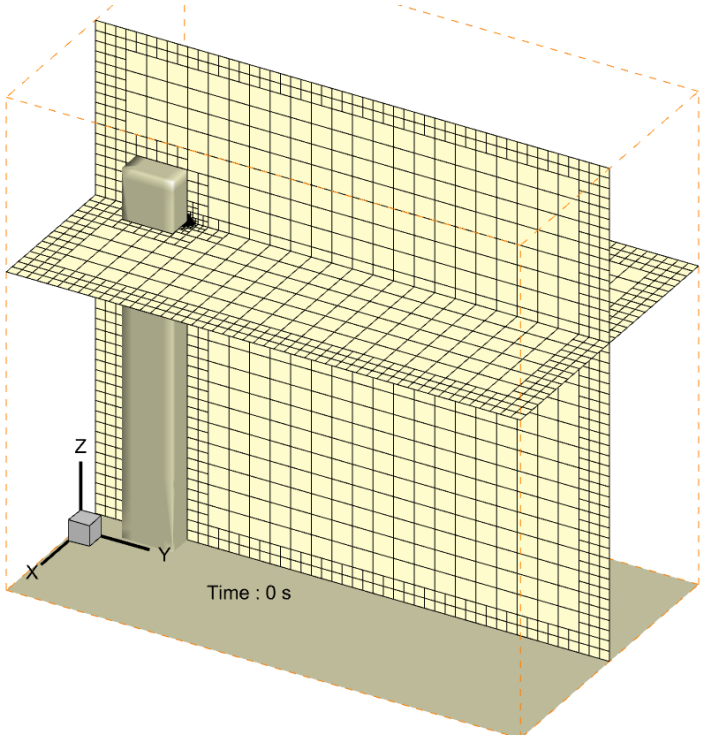

FIGURE 24 INITIAL GRID AT 0 SECONDS WITH FIXED EMBEDDING

The snapshot above shows grid in the vertical and horizonal direction in the y-z and x-y planes. The slices placement is in the centre of the mouth. The timestamp is at zero seconds, just at the base of the simulation. Notice the fixed embedding that occur around the wall and mouth area. This is the specification that this are the critical locations.

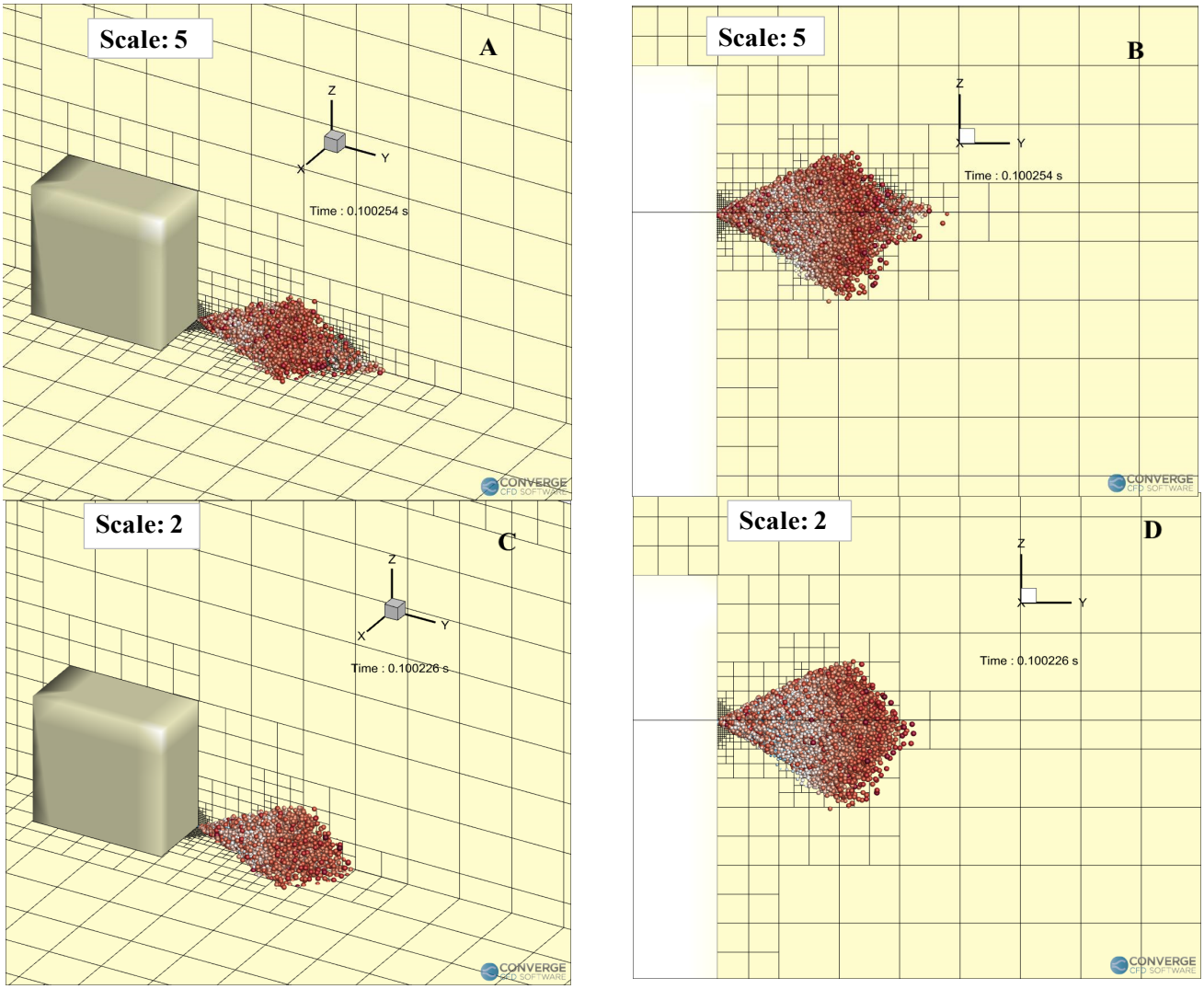

FIGURE 25 DIFFERENCE IN AMR AFTER 0.1 S IN X-Y AND Y-Z-PLANE

The figure 25 shows the similar view angle and time of cough simulations with different AMR settings. As the cough particles eject the dynamic evolution of the adaptive mesh refinement activates. The changes in size and number the black rectangular boxes which represents the grid, adjust according to the multiphase fluid flow. By looking at the grid resolution we can see that illustration A and B have a finer resolution than C and D, that use the lowest scaling factor. See next figure for clearer difference.

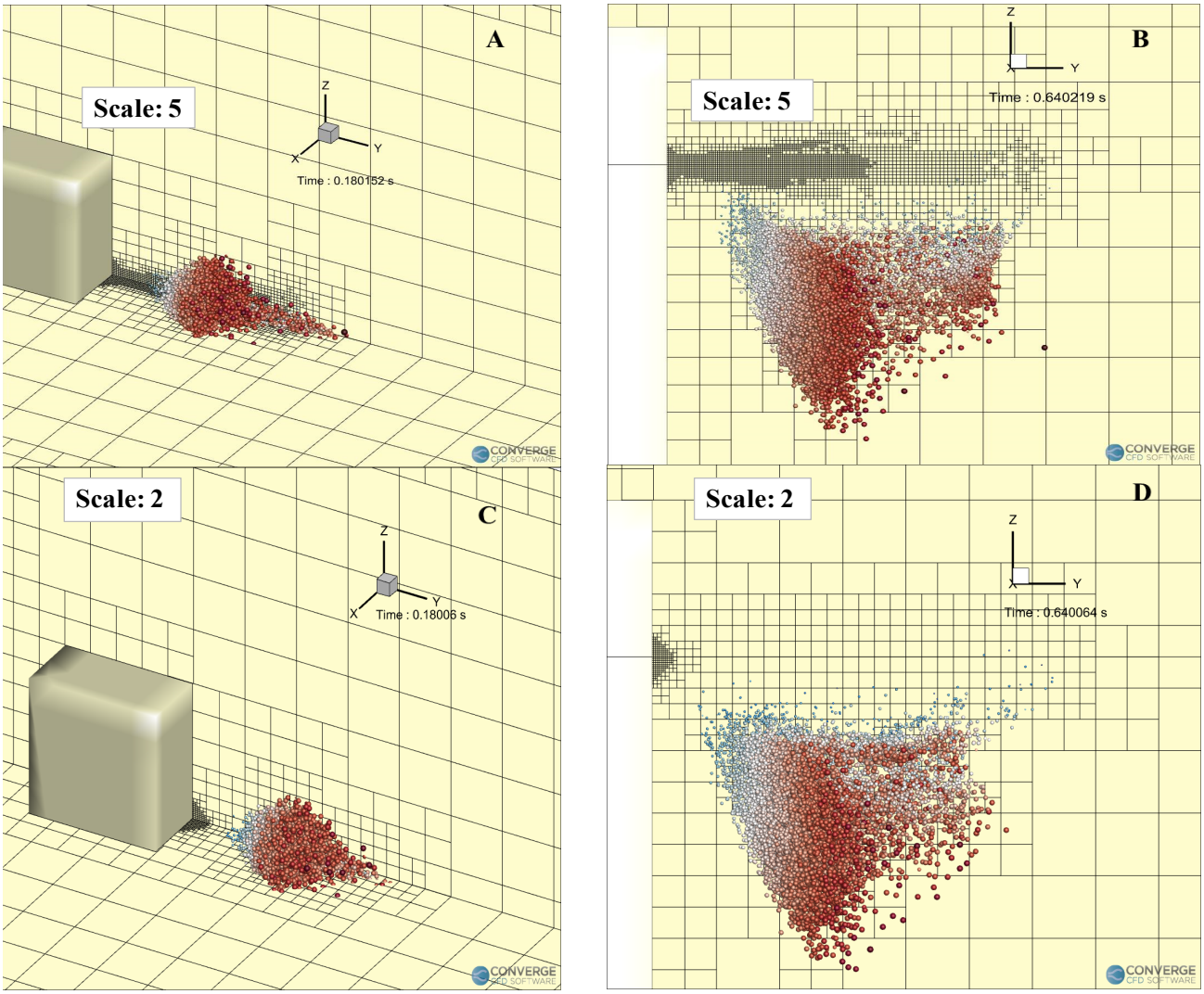

FIGURE 26 COMPARISON OF AMR SCALING AFTER 0.18 S. AND 0.64 S. IN X-Y -AND Y-Z-PLANE

As the timeline of a cough continues it becomes more obvious how the automatic grid resolution work. After 0.18 sec picture A (figure 26), already have a relatively fine mesh around cough droplets and it continues to fluctuate with the multiphase flow as shown in B after 0.64 sec, even though at this point the bigger droplets starts to fall towards the ground. C and D have lower resolution as dictated by the AMR setting.

To put this into context regarding simulation time, the cases are simulated on the same computer, but the higher resolution have a simulation time that is 180% higher compared to the lower AMR simulation.

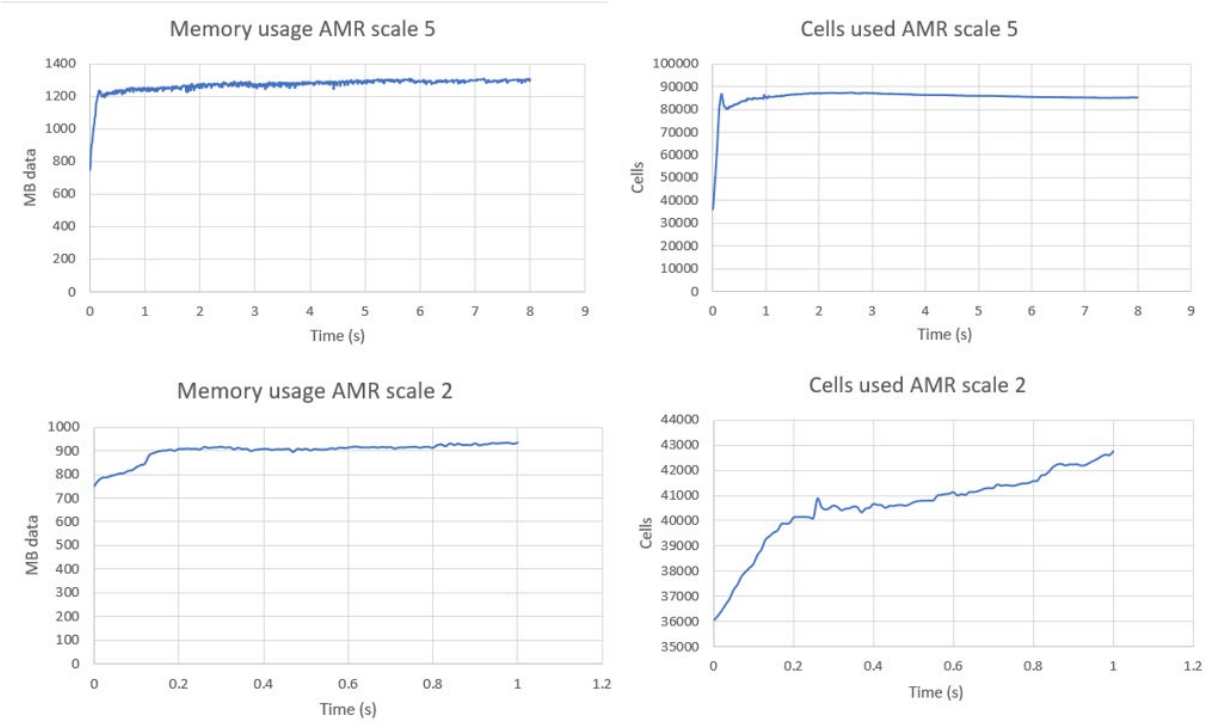

FIGURE 27 ILLUSTRATIN OF MEMORY USE AND CELLS USED REGARDING DIFFERENT AMR SETTINGS. TIME SCALE REPRESENTS 1-8 SECONDS IN ALL FOUR PICTURES

A comparison for the same 8 seconds simulation is shown above. Here the time and computer power used for the two simulations is presented in terms of memory usage per second and cells used per second. Even the compared tests have different simulation time, the difference is representative for the change in grid resolution.

The general value of the AMR function will most likely save both time and money compared to a manual made grid because the simulating will focus the finer grid on the chosen critical area instead of a manually made grid which most other CFD software offers.

4.3 CHANGE IN PARTICLES, CASE 1, 3 & 4

In this section the change in particles numbers is our variable. The same total mass of injection is the same for all cases, but the number of particles vary.

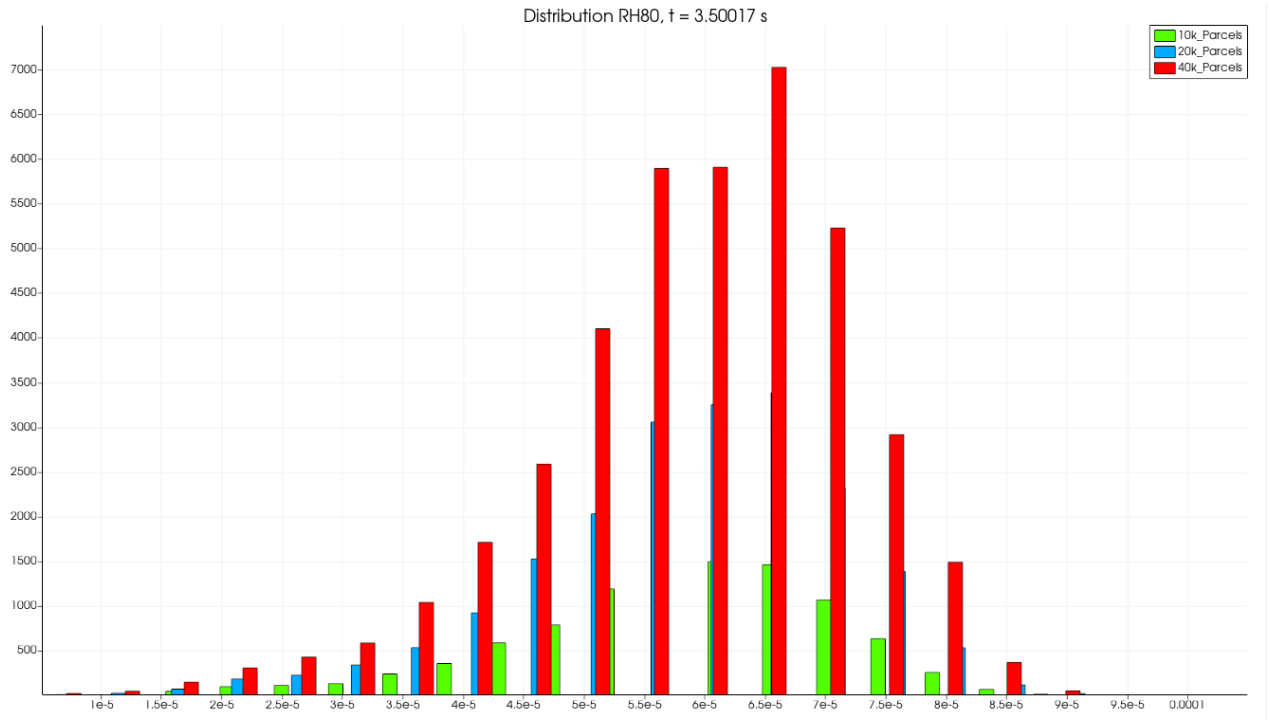

FIGURE 28 DISTRIBUTION WITH CHANGE IN PARTICLES

For three cases with 10 000, 20 000 and 40 000 parcels we almost have the similar nature of the distribution (figure 28). As there is a shift in number of droplets, the peak value of parcels will obviously have higher number on the distribution with most particles. The peak in droplet size is approximately in the same area for all tree cases, with a value of 65 μm.

The SMD value for the three cases are almost similar with 63 μm for 10 000 parcels, 67.5 μm for 20 000 and 63 μm for 40 000 parcels. This is reasonable as SMD represents the diameter of a droplet whose ratio of volume to surface area is equal to the entire cough spray. See figure 47, figure 48 and figure 49 in attachment for more info.

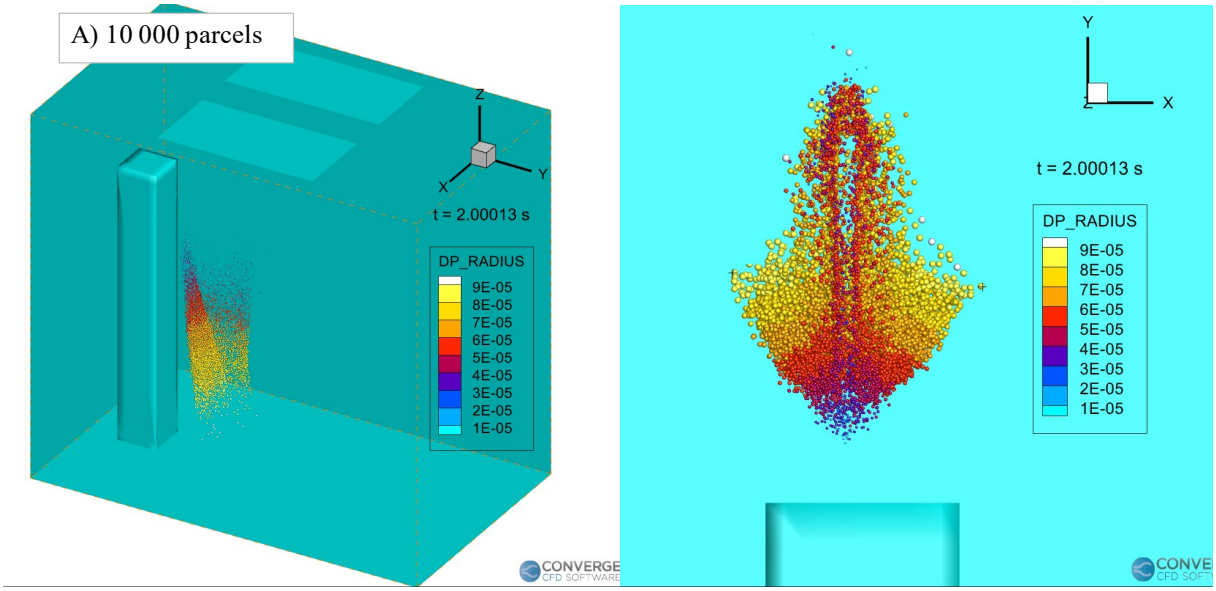

FIGURE 29 PARTICLES SPREAD WITH 10 000 PARTICLES

Figure 29 show a still picture of a cough after 2 seconds with 10 000 injected parcels. The distance in the y-direction is 0.75m and the spread at this point are 0.315 m.

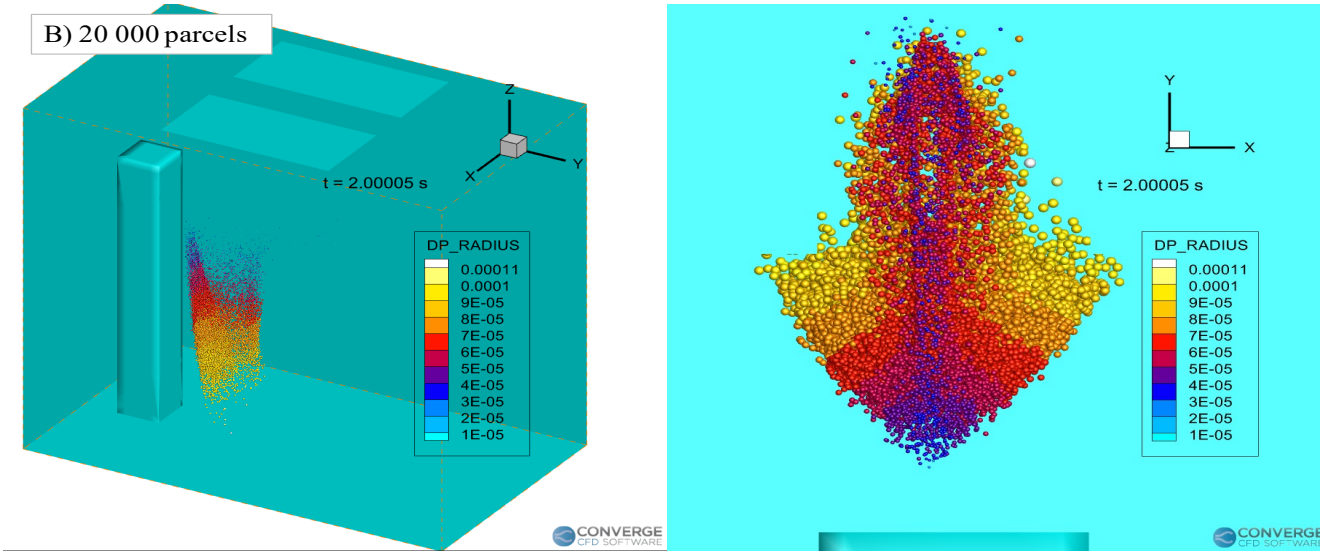

FIGURE 30 PARTICLES SPREAD WITH 20 000 PARTICLES

Figure 30 show a still picture of a cough after 2 seconds with 20 000 parcels injected. The distance in the y-direction is 0.75m and the spread at this point are 0.33 m.

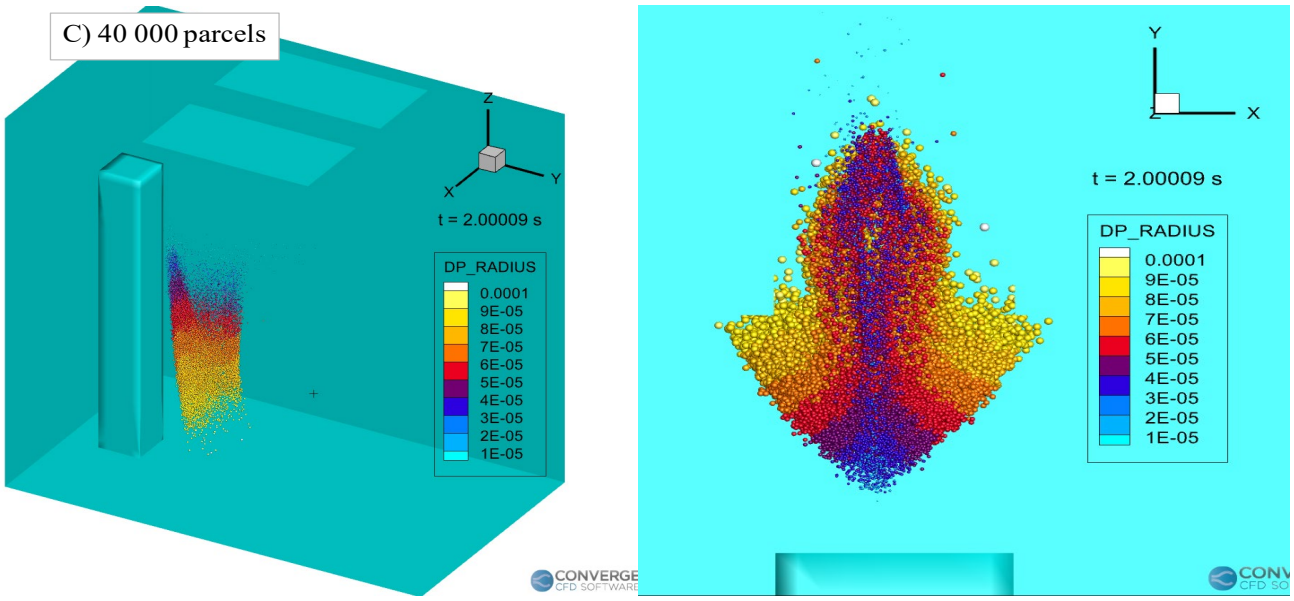

FIGURE 31 PARTICLES SPREAD WITH 40 000 PARTICLES

Figure 31 show a still picture of a cough after 2 seconds with 40 000 parcels injected. The distance in the y-direction is 0.75m and the spread at this point are 0.35 m. As the cloud shows, we can see a change in the cloud size due to more parcels. Since the ejected mass is the same for all three cases, we notice that the distribution are almost the same for the three cases, see figure 28, with the only change in amount of parcels (y-axis). Since its reasonable to assume the results are independent of number of droplets and the fact that including more particles are statistically more reliable, we notice that only (D'Alessandro et al., 2021) and (Zhou & Ji, 2021) used an number of particles above 20000, this point out the challenge due to computational simulating such a complex flow physics.

4.4 CHANGE IN RELATIVE HUMIDITY, CASE 5 & 6

In this section, we present the effect of relative humidity of human cough instances on the elevator setup. We simulated case 5 and 6 with RH of 40% and 80%.

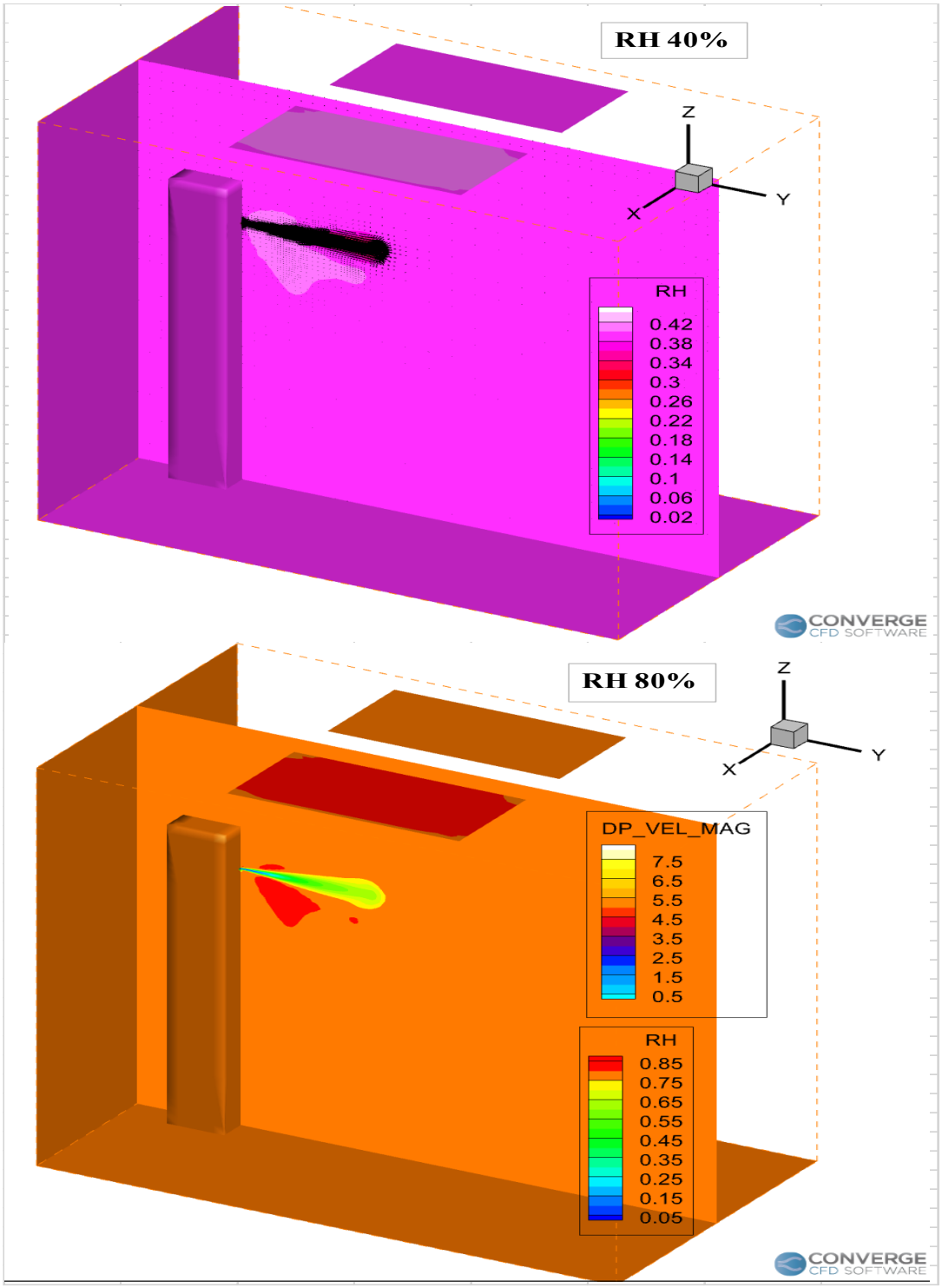

FIGURE 32 CHANGE IN RELATIVE HUMIDITY. VALUE-SCALE CONFIRM OUR INPUT SETTINGS

It is evident from the figure 32 that the RH distributions are in accordance with the considered initial conditions for cases 5 and 6. The velocity vectors of the exhaled gas arising from cough instance and droplet velocity magnitudes are also shown in figure 32. Note that the amount of evaporation is considerably smaller than the existing water vapor content in the surrounding moist air in the confined space. This is proven trough the RH color scale in both simulations. In addition to this we can see in the top section of the picture velocity vectors from the mouth, and the bottom section include the parcels velocity magnitude.

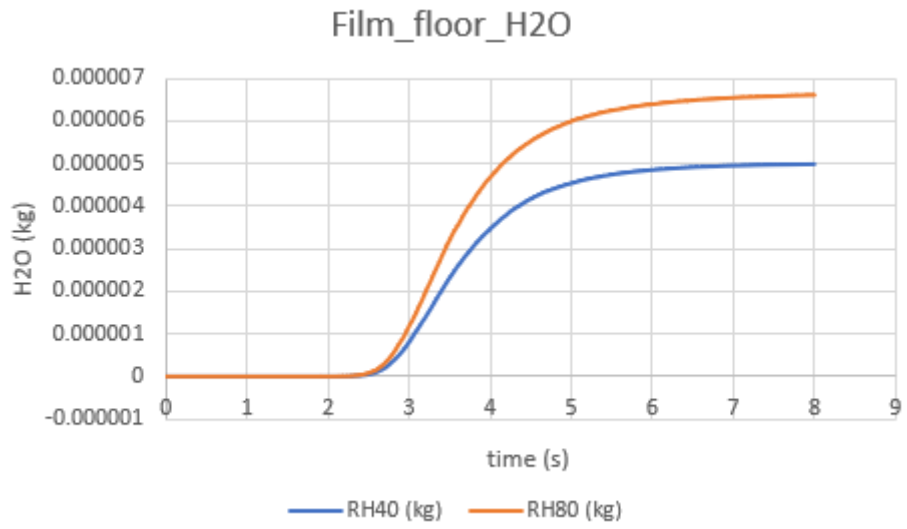

FIGURE 33 MASS H2O ON FLOOR FROM COUGH OVE RTIME

The diagram above shows the evolution of mass of liquid H2O on the floor during the simulation period for 8 seconds for both RH40 (case 5) and RH80 (case 6). From the initial 7.7 μg ejected mass, we see a change in how much mass of water that ends up on the elevator floor. At the end of the simulation, the case with RH40 results in 5 μg on the ground, against 6.7 μg from the RH80 case. This further reveals the amount of evaporation from the injected liquid mass for each case. The case with the lowest relative humidity has the highest evaporation rate, which seems natural. This is confirmed in (Feng et al., 2020) where they conclude that a lower RH triggers the evaporation in cough droplets, which again leading to droplet size reduction and therefore may lead to a longer time suspended in the air. (Sen, 2021) show an

evaporation rate for a similar case with RH 30% to be approximately 75%, which is higher that our rate for the RH40. If we assume all the mass that does not fall to the ground, evaporates, we get an evaporation of nearly 35%. This difference can be related to differences in several input parameters and models used in the simulations. Further deeper extensive analysis is required to conclude on this.

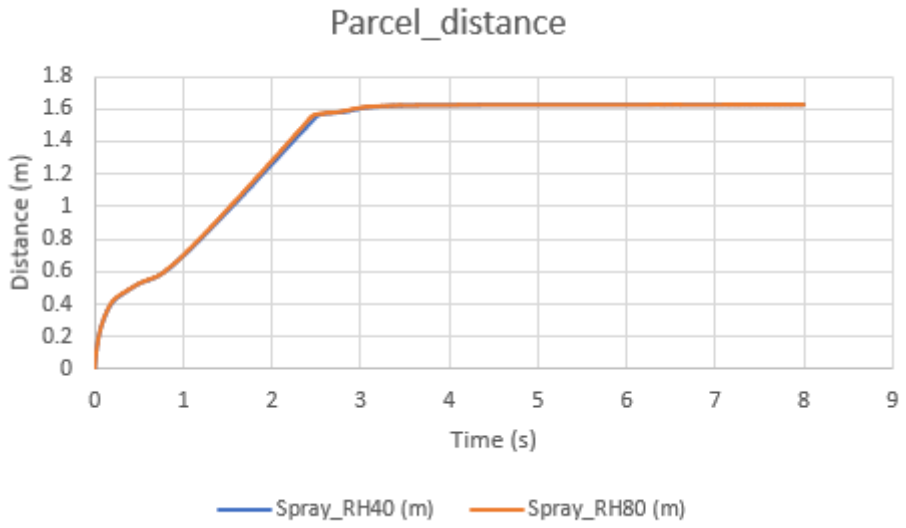

FIGURE 34 TRAVEL LENGTH DROPLETS FROM COUGH

Figure above show the travel distance to the bigger droplets before gravity pulls them to the ground. And here we can see for both cases that before the last droplets hits the floor, they have travelled nearly 1.6m from the host. As most governments recommend a minimum distance of 1 meter to stay in a safe zone this is critical at first sight.

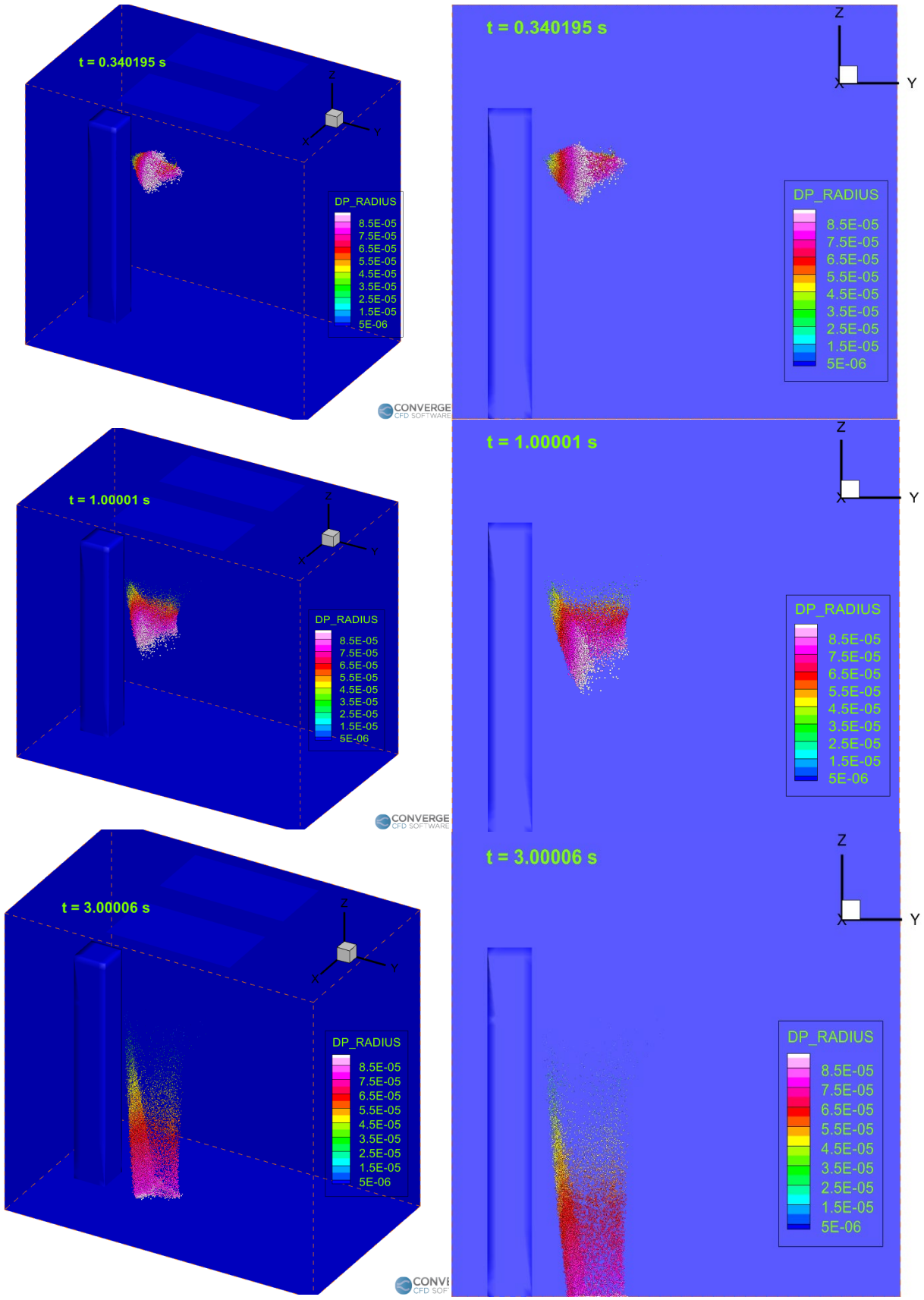

FIGURE 35 TIMESNAPS OF X-Y AND Y-Z-PLANE FOR DROPLET FALL

Figure 35 shows time-snaps for one cough with belonging droplets and here we see that already from 1 second after cough the droplets have fallen relatively much if compared to our 1.80m tall human. So, for the contaminated area connected to the droplets, we can assume that even the distance exceeds 1 meter, at that point the droplets are only around 1m. above the ground and not in the breathing zone of eventual other standing humans in the elevator. Our results are relatively similar to some of the articles mentioned in section Literature 1.3, which tells us that the travelled distance in (D'Alessandro et al., 2021) was found have max length of 1.8m while (Dbouk & Drikakis, 2021) found the distance to be approximately 1.7m. The results of the presented simulations are in accordance with these studies.

4.5 ANALYSE OF THE EVOLUTION OF THE LIQUID PHASE SIZE DISTRIBUTION

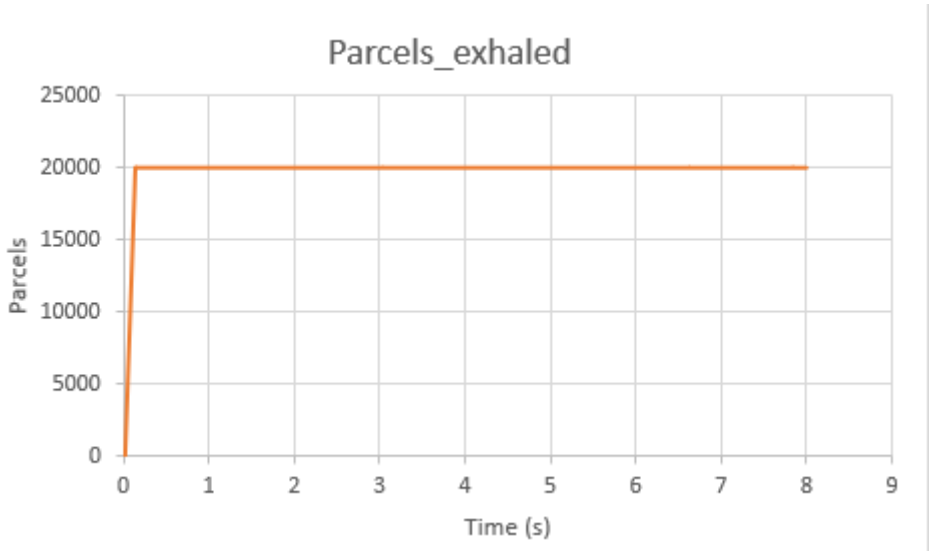

FIGURE 36 RATE PARCELS INJECTION

As previously illustrated in figure 13, figure 36 show the injection rate of the cough parcels.

Case with Relative humidity at 40 %

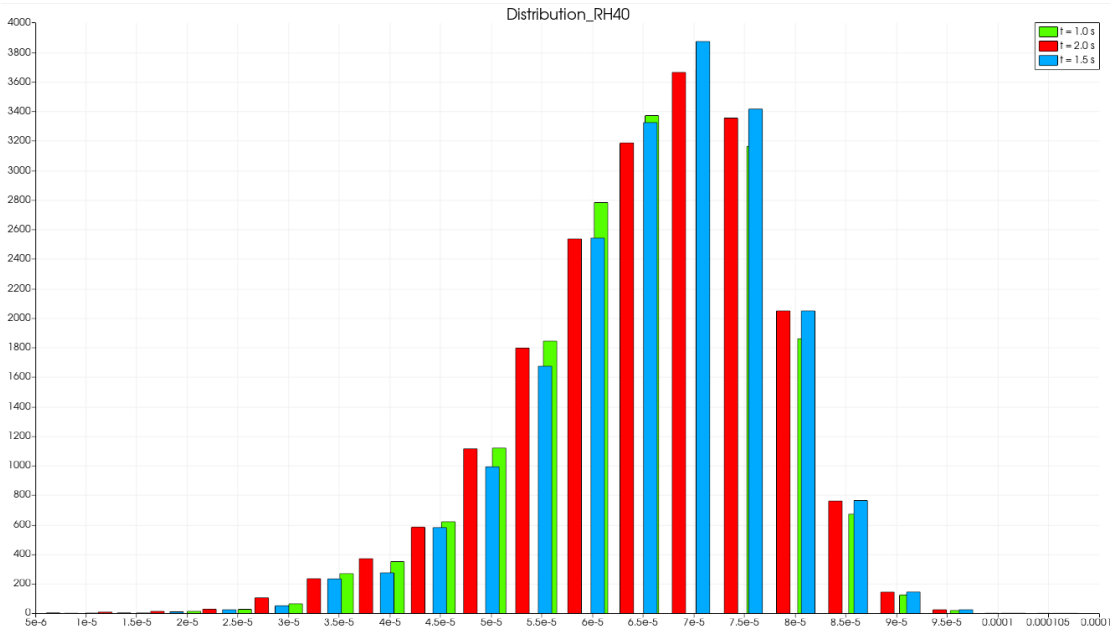

FIGURE 37 DISTRIBUTION RH40 FROM 1-2 SECOND

aboveFigure 37 shows the distribution between 1-2 seconds for case 5. In the histogram above, we can see most values will be around 70μm. The distribution ranges between 13 – 95 μm

parcels. It can be notice that there is a marginal shift of the distribution towards the higher size range at later times. The change in the distribution is linked with the evaporation and other droplet-droplet interactions during the evolution of the flow-field.

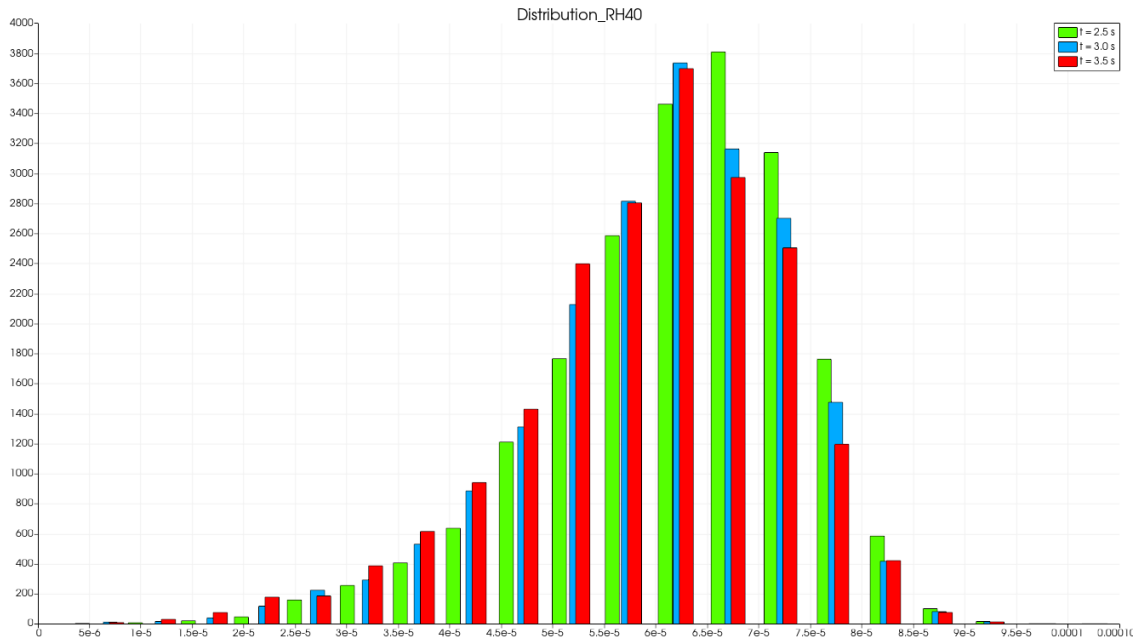

FIGURE 38 DISTRIBUTION RH40 FROM 2.5-3.5 SECONDS

Figure 38 shows the next period in the simulation, 2-3.5s. Similar happens here as in the previously time period. The peak is around 63 μm. Our SMD value at 2.5 seconds are 67 μm.

Case with Relative humidity at 80 %

Here we present the case with relative humidity 80% at similar time instants as before.

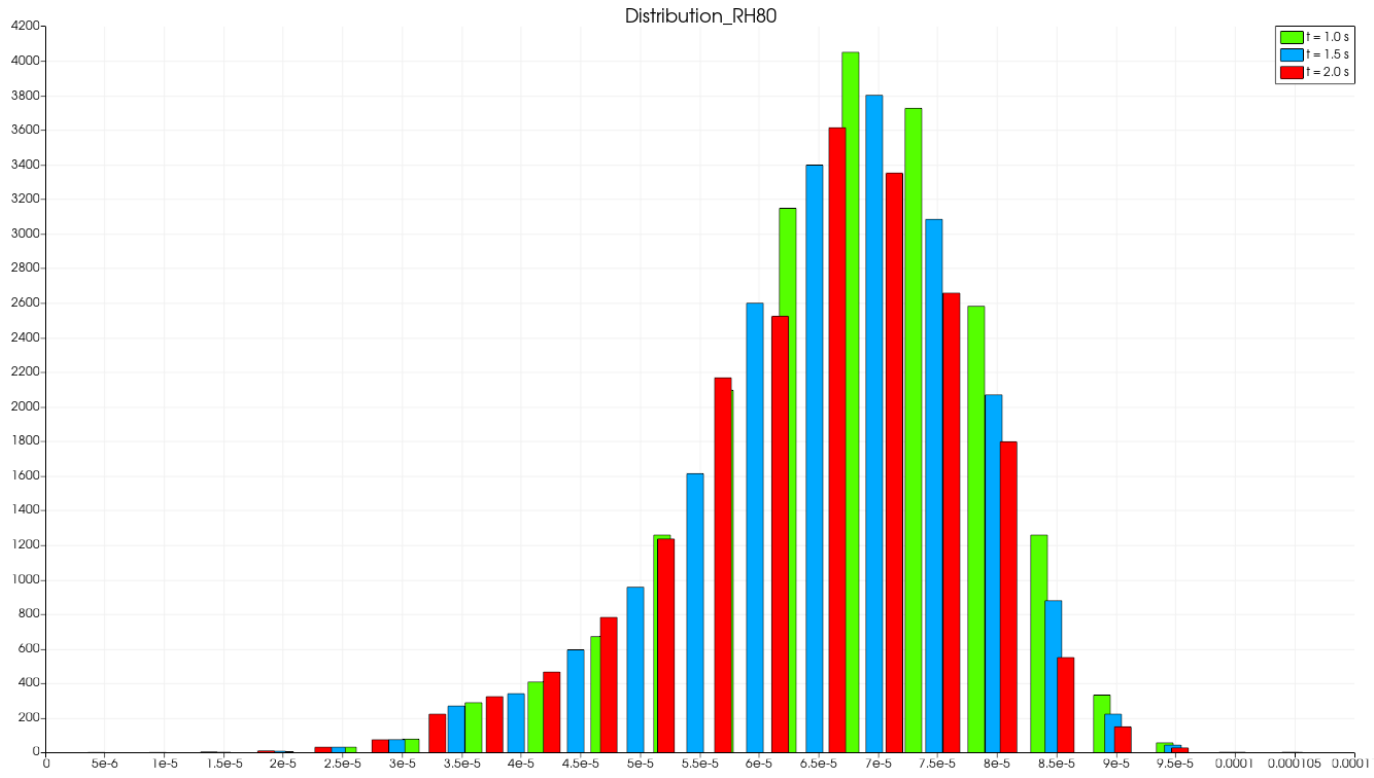

FIGURE 39 DISTRIBUTION FOR RH 80 FROM 1.0-2.0 SECONDS

For 1-2s, figure 39, the distribution has a peak of around 67 μm with a shift towards the right. The values lie between 15 - 95 μm and also here we can see that it looks like the smaller droplets are lesser than the bigger droplets.

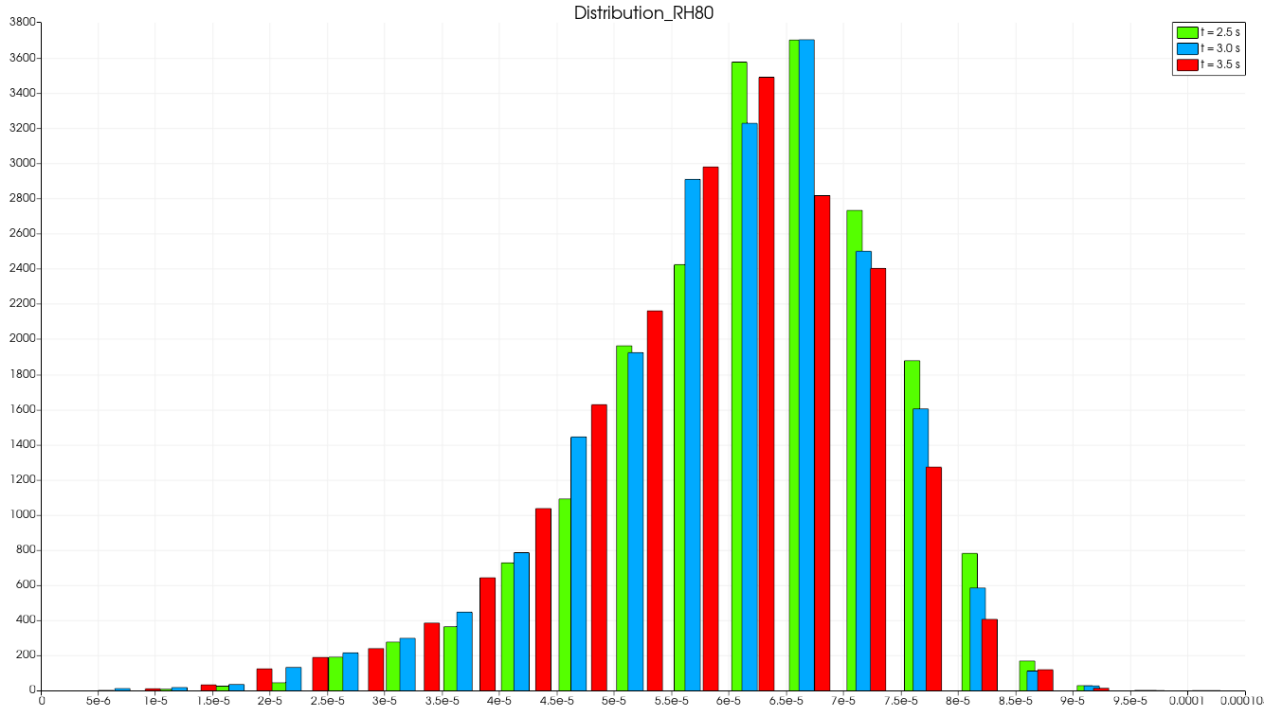

FIGURE 40 DISTRIBUTION RH 80, 2.5-3.5 SECONDS

Figure above shows the next period in the simulation, 2-3.5s. Similar happens here as in the previously time period. The peak is around 68 μm. And since it is after a longer time than figure 23, the change in the peak value can be because of evaporation where the smaller droplets change to the gaseous phase. In this regard, the recent study of (D'Alessandro et al., 2021) reported a similar trend of the dynamics of liquid phase size distribution considering 4900 lquid parcels where the cough droplets are irradiated by ultraviolet-C light.

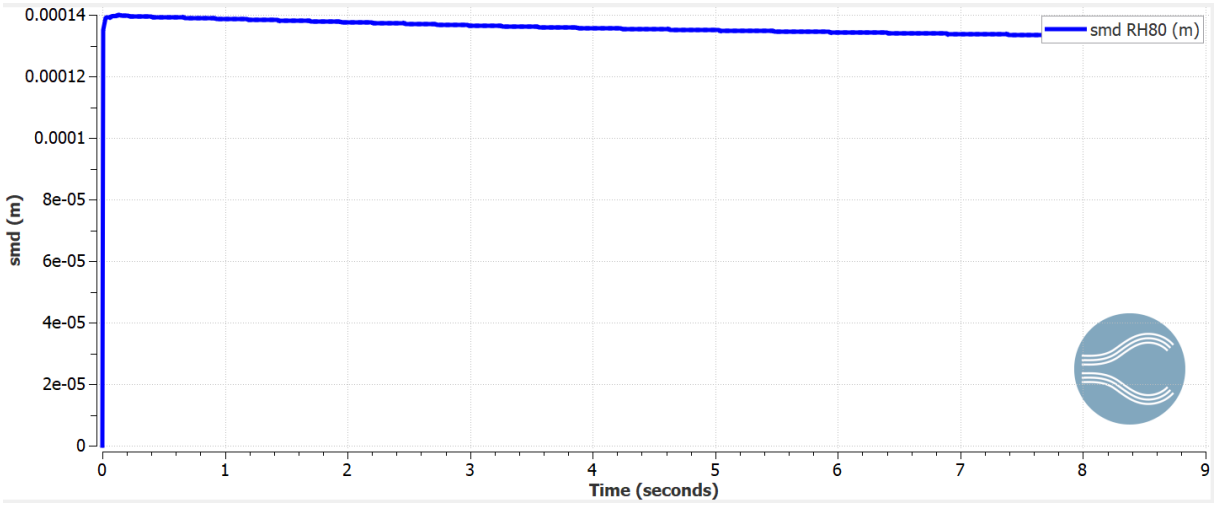

FIGURE 41 SMD FOR RH 80% SIMULATION

Figure 41 shows the SMD (see Table 7) for our simulation case with 80% RH. Here we see that we have a sauter mean diameter after 4 seconds $\frac{135}{2}$ μm (our radius), which is 67.5 μm. This corroborates very well when we compare our mean with (D'Alessandro et al., 2021) who had a value of 68 μm after four seconds of simulating.

Distribution with change in RH

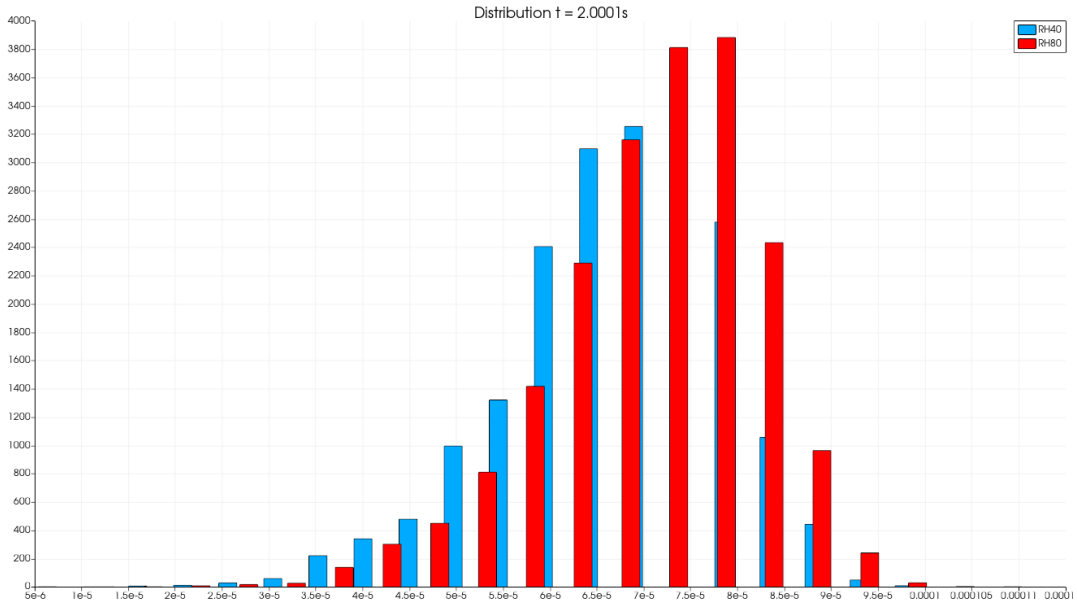

FIGURE 42 COMPARISON OF DISTRIBUTION DUE TO CHANGE IN RH

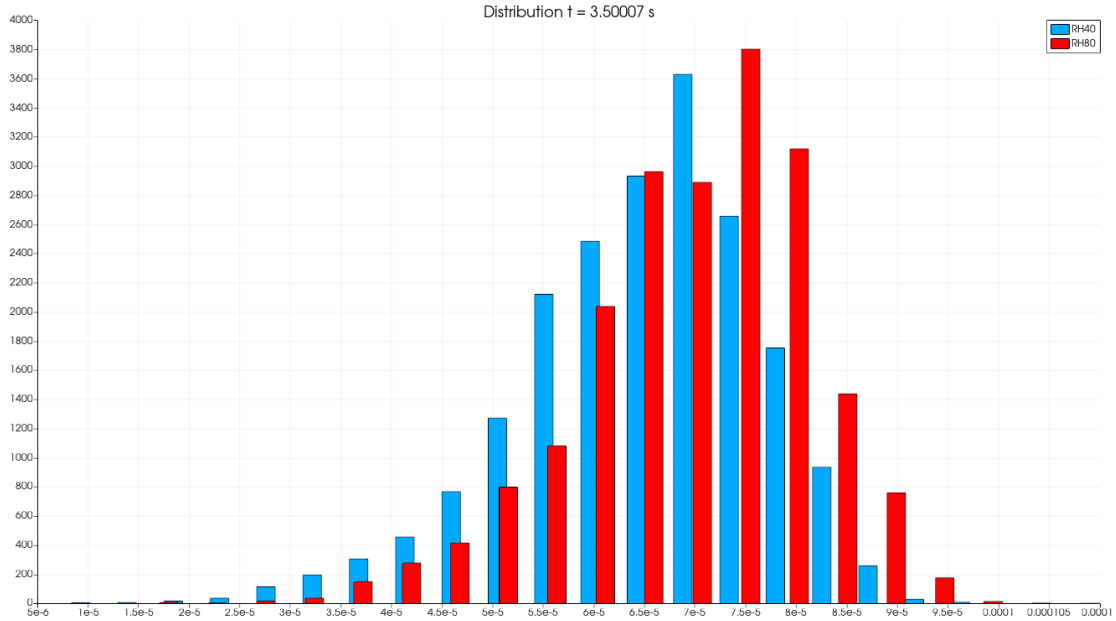

FIGURE 43 COMPARISON OF DISTRIBUTION DUE TO CHANGE IN RH

Figure 42 and figure 43 show time snaps of the distribution curves with varying relative humidity. We can see here the same pattern as the distribution in the section above. A marginal shift to the right. The difference we can notice is the change in peak value for these cases. In

figure 41, RH 40 have a peak at 73 μm while RH 80 peak at 80 μm after 2 seconds. For figure 42 which is 3.5 seconds of the simulation, RH 40 have a peak at 69 μm while RH 80 peak at 75 μm. A shift to the left between the time snaps.

In this report, we presented the general characteristics of the space-time evolution of the parcel size distribution. A detailed analysis of the evolution of the size distribution could be performed by varying several input parameters for deeper understanding of the underlying heat and mass transfer mechanisms associated with the prevailing turbulent multiphase flow in indoor environments.

5 CONCLUSIONS

In this work, we have revisited the human cough instances in an elevator setup with advanced 3-dimensional AMR based multiphase flow simulations. For this, first a brief literature review has been performed considering experimental findings as well as the numerical works utilizing Eulerian-Lagrangian multiphase solution techniques. The present work makes use of the computationally effective AMR method to resolve unsteady complex flow physics involving heat and mass transfer in a turbulent multiphase flow. The Eulerian dispersion medium is considered as a multicomponent ideal gas mixture consisting of O2, N2 and H2O and the Lagrangian dispersed phase of human cough is considered as pure liquid water. A simplified rectangular block model is used to mimic a human being in a standing position and a rectangular mouth area is considered for injecting exhaled gas and liquid droplets associated with cough instances.

We first demonstrated the mode of operation of the AMR based methodology by Case 1 and 2. The results of these cases show the benefit of the usage of AMR based techniques for resolving the flow characteristics of the complex multiphase flow. Additionally, the efficacy of the usage of liquid phase size distribution has been studied by varying the number of liquid parcels in the simulation cases 3 and 4. The results are found to be independent of the number of droplets considered in the simulations. Furthermore, the effect of RH is investigated with fixed ACH in a realistic elevator setup in cases 5 and 6. The results show about 35% evaporation for RH of 40% for 7.7 μg liquid injection for cough instance. An analysis of the dynamics of the liquid phase size distribution, penetration length and spread are presented, and the results are found to be in accordance with a very recent research article.

Future work

Several simulations have been performed originally but omitted from the results section due to unintentional inappropriate boundary conditions. These are noticed at the later stage of the project and therefore limited the total number of numerical cases presented in the report. A few numerical challenges with the case setup as the physics is complex, because of the multiphase flow, some simplifications are made. The saliva droplets are modelled with pure liquid water, which in reality will be a salt solution. The human body used in the elevator are interpreted like a rectangular box, and the thermal plume from the body is not considered. Other workings on the same things parallelly so several new findings have been reported during the working phase of this project/work

The unexplored method of involving CFD simulations to analyze and understand how airborne viruses behave in different scenarios with change in variations can still evolve. As results in this thesis shows there is further work needed at some areas to be able to understand and predict how multiphase airflow affects humans in indoor climate. Some suggestions, that this thesis did not have the time for but could be done, is make the modelling more realistic. Both geometry and thermal property. For example, adding breathing sequence in between coughs, adding more humans to the simulation. Moreover, motion with head or body and door opening sequence in the elevator could also be investigated. One can perform several parametric and sensitivity analyses by varying relevant parameters.

.

6 REFERENCES

Busco, G., Yang, S. R., Seo, J. & Hassan, Y. A. (2020). Sneezing and asymptomatic virus transmission. *Phys Fluids (1994)*, *32*(7), 073309. https://doi.org/10.1063/5.0019090

Cengel, Y. A. & Ghajar, A. J. (2015). *Heat and Mass Transfer, fundamentals and applications* (5th. utg.). McGrawHill Education.

D'Alessandro, V., Falone, M., Giammichele, L. & Ricci, R. (2021). Eulerian-Lagrangian modeling of cough droplets irradiated by ultraviolet-C light in relation to SARS-CoV-2 transmission. *Physics of Fluids*, *33*(3). https://doi.org/Artn 031905

10.1063/5.0039224

Dbouk, T. & Drikakis, D. (2020a). On coughing and airborne droplet transmission to humans. *Physics of Fluids*, *32*(5). https://doi.org/Artn 053310

10.1063/5.0011960

Dbouk, T. & Drikakis, D. (2020b). On respiratory droplets and face masks. *Phys Fluids (1994)*, *32*(6), 063303. https://doi.org/10.1063/5.0015044

Dbouk, T. & Drikakis, D. (2021). On airborne virus transmission in elevators and confined spaces. *Phys Fluids (1994)*, *33*(1), 011905. https://doi.org/10.1063/5.0038180

Feng, Y., Marchal, T., Sperry, T. & Yi, H. (2020). Influence of wind and relative humidity on the social distancing effectiveness to prevent COVID-19 airborne transmission: A numerical study. *J Aerosol Sci*, *147*, 105585. https://doi.org/10.1016/j.jaerosci.2020.105585

Greenhalgh, T., Jimenez, J. L., Prather, K. A., Tufekci, Z., Fisman, D. & Schooley, R. (2021a). Ten scientific reasons in support of airborne transmission of SARS-CoV-2. *Lancet*, *397*(10285), 1603-1605. https://doi.org/10.1016/S0140-6736(21)00869-2

Greenhalgh, T., Jimenez, J. L., Prather, K. A., Tufekci, Z., Fisman, D. & Schooley, R. (2021b). Ten scientific reasons in support of airborne transmission of SARS-CoV-2 (vol 397, pg 1603, 2021). *Lancet*, *397*(10287), 1808-1808. <Go to ISI>://WOS:000651041900023

Gupta, J. K., Lin, C. H. & Chen, Q. (2009). Flow dynamics and characterization of a cough. *Indoor Air*, *19*(6), 517-525. https://doi.org/10.1111/j.1600-0668.2009.00619.x

Law of the wall. [Fluid dynamics, turbulence]. Wikipedia, Wikipedia, the free encyclopedia. https://en.wikipedia.org/wiki/Law_of_the_wall

Malalasekera, H. K. V. W. (2007). *An introduction to computational fluid dynamics: The finite volume method* (Second edition. utg.). Person Education Ltd.

science, C. (2021). *Converge cfd manual series, Converge manual* (3.0. utg.). Converge Science. https://hub.convergecfd.com/downloads/category/22-documentation#

Sen, N. (2021). Transmission and evaporation of cough droplets in an elevator: Numerical simulations of some possible scenarios. *Phys Fluids (1994)*, *33*(3), 033311. https://doi.org/10.1063/5.0039559

Versteeg, H. K. & Malalasekera, W. (2007). *An introduction to computational fluid dynamics: The finite volume method* (Second edition. utg.). Person Education Ltd.

Vömel, H. (2016). *Arden Buck equation, Saturation vapor pressure formulations*. National Center for Atmospheric Research. http://cires1.colorado.edu/~voemel/vp.html

WHO. *World Health Organization*. https://www.who.int/emergencies/diseases/novel-coronavirus-2019/advice-for-public

Zafra, M. (2020, 20.10.2020). A room, a bar and a classroom: how the coronavirus is spread through the air. *El Pais*.

Zhou, Y. & Ji, S. (2021). Experimental and numerical study on the transport of droplet aerosols generated by occupants in a fever clinic. *Building and Environment*, *187*. https://doi.org/ARTN 107402

10.1016/j.buildenv.2020.107402

Zhu, S. W., Kato, S. & Yang, J. H. (2006). Study on transport characteristics of saliva droplets produced by coughing in a calm indoor environment. *Building and Environment*, *41*(12), 1691-1702. https://doi.org/10.1016/j.buildenv.2005.06.024

7 ATTACHMENT

TABLE 8 CALCULATION SPECIES FRACTION

	A	B	C
1			
2	T_{supply}	21	°C
3	RH Oslo	80	%
4	M_M Air	28.97	kg/kmol
5	M_M H_2O	18.015	kg/kmol
6	$P_{elevator}$	101325	Pa
7			
8	Saturated vapor pressure		
9	P_{sat}	2.487160911	kPa
10	P_{vapor}	1989.728728	Pa
11			
12	Fraction vapor/air		
13	Υ_{vapor}	0.019637096	
14	Υ_{air}	0.980362904	
15			
16	Fractions		
17	ω_{vapor}	0.012302689	
18	ω_{air}	0.987697311	
19			
20	ω_{O_2}	0.230133474	
21	ω_{N_2}	0.769866526	
22		**Mass fraction**	
23	$\boldsymbol{H_2O}$	0.012302689	
24	$\boldsymbol{O_2}$	0.227302213	
25	$\boldsymbol{N_2}$	0.760395098	
26	sum	1	
27			
28	$P_s(T) = 6.1121 \exp\left(\left(18.678 - \frac{T}{234.5}\right)\left(\frac{T}{257.14+T}\right)\right)$		
29			
30	$\omega_{O_2=0.233}\omega_{air}$		

TABLE 9 CALCULATION OF SPECIES FRACTION WITH FORMULAS

	A	B
1		
2	T_{supply}	21
3	RH Oslo	80
4	M_M Air	28.97
5	M_M H_2O	18.015
6	$P_{elevator}$	101325
7		
8	Saturated vapor pressure	
9	P_{sat}	=0.61121*EKSP((18.678-(B2/234.5))*(B2/(257.14+B2)))
10	P_{vapor}	=1000*(B3*B9/100)
11		
12	Fraction vapor/air	
13	Υ_{vapor}	=B10/B6
14	Υ_{air}	=1-B13
15		
16	Fractions	
17	ω_{vapor}	=(B13*B5)/(B13*B5+B14*B4)
18	ω_{air}	=1-B17
19		
20	ω_{O_2}	=0.233*B18
21	ω_{N_2}	=1-B20
22		**Mass fraction**
23	$\boldsymbol{H_2O}$	=B17
24	$\boldsymbol{O_2}$	=B18*B20
25	$\boldsymbol{N_2}$	=B18*B21
26	sum	=B23+B24+B25
27		
28		
29		
30		

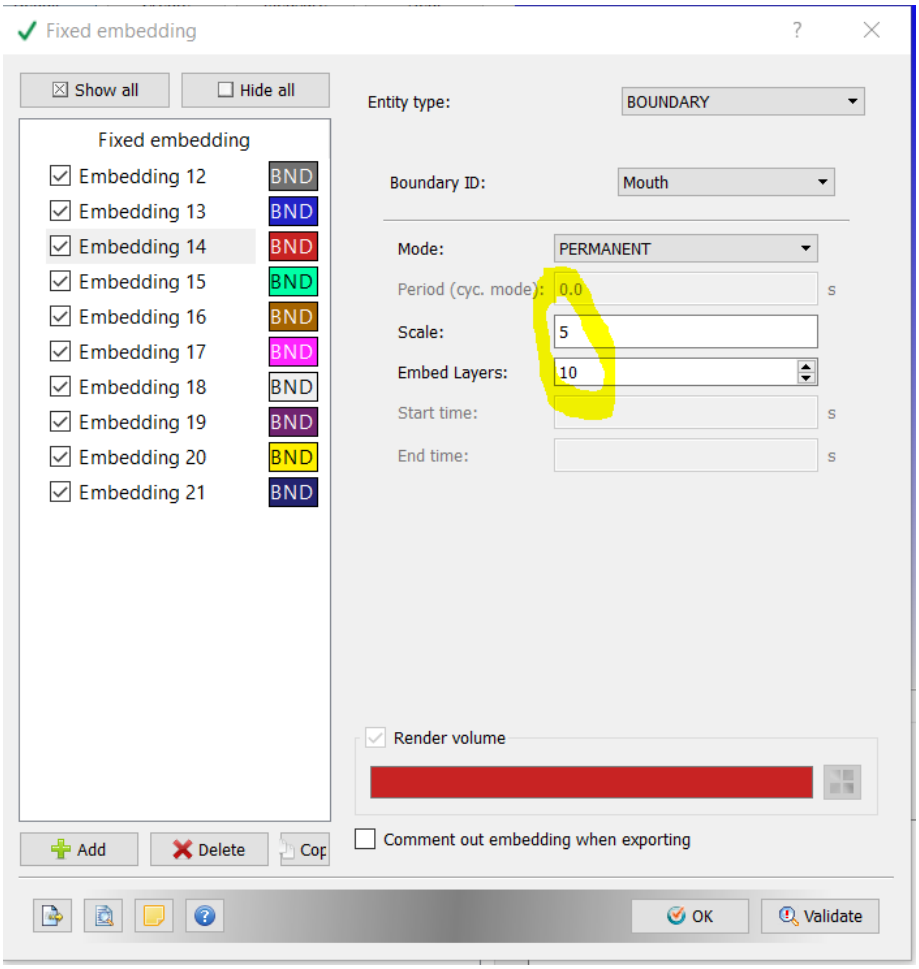

FIGURE 44 EMBEDDING SETTING IN MOUTH/NOZZLE AREA

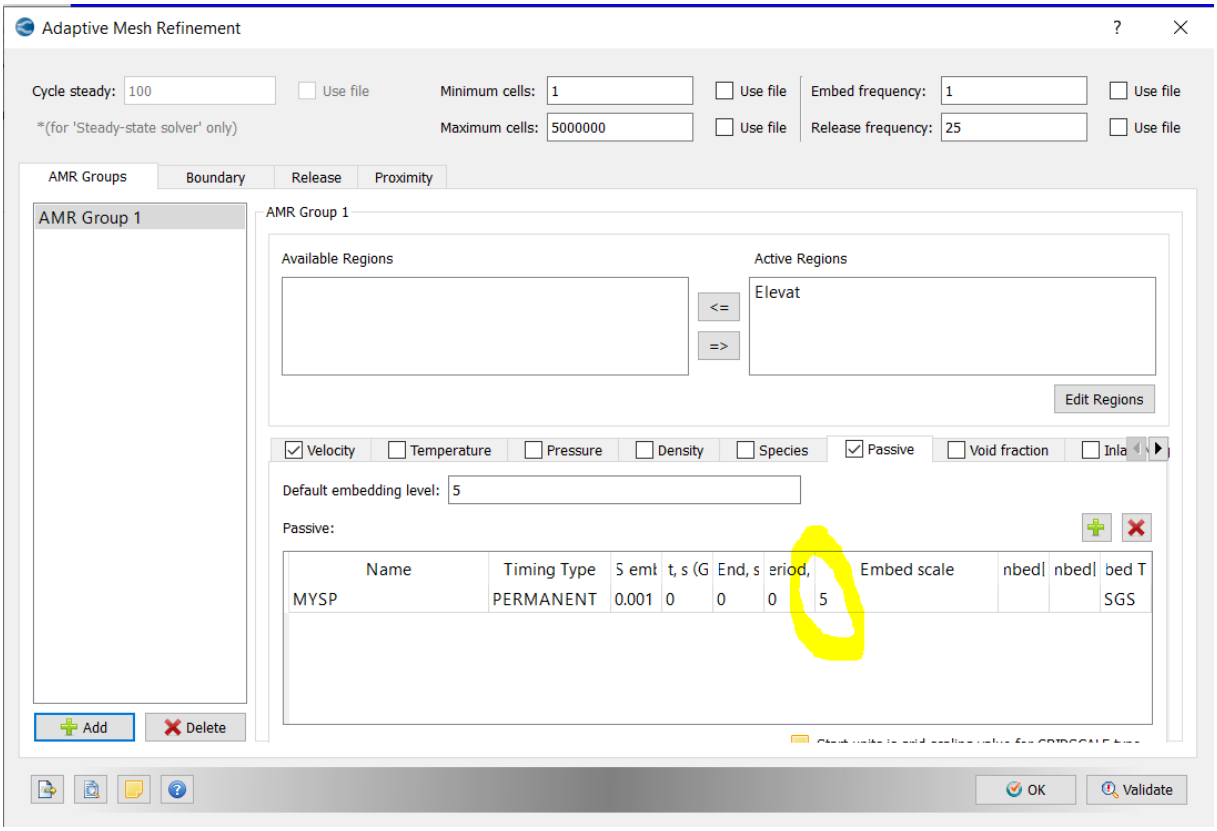

FIGURE 45 AMR SETTING MOUTH AREA

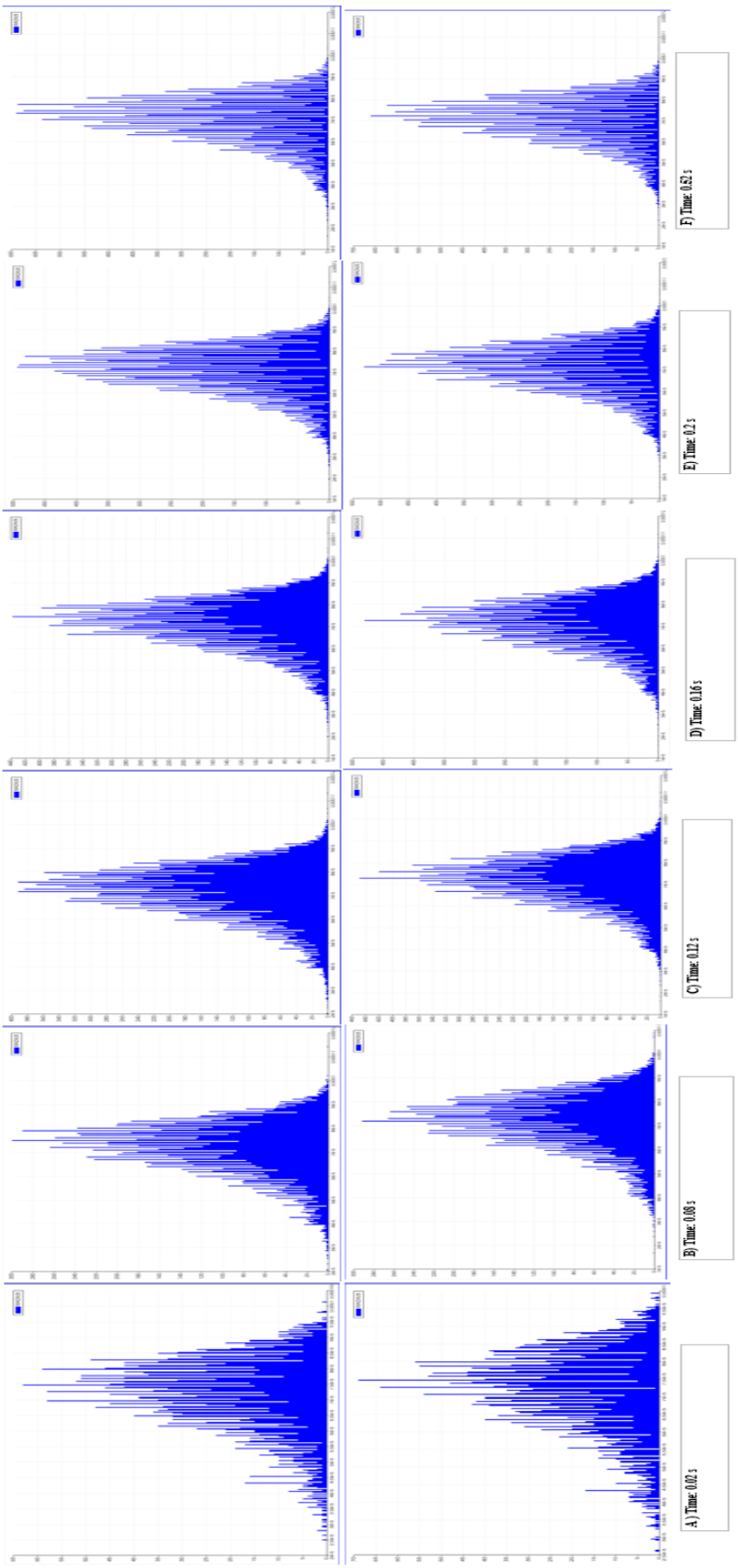

FIGURE 46 TIMESNAPS OF DISTRIBUTION RH80 (ABOVE) AND RH40 (BELOW). THE TIME SNAPS ARE MARKED UNDER AND SHOWS VARIOUS TIME, TO GET AN OVERVIEW ABOUT HOW THE DISTRIBUTION SHIFT. THE BIN SIZE ARE HIGH BUT WE CAN SE A SLIGHTLY SHIFT TO THE RIGHT OVER TIME. AS MENTIONED BEFORE, THIS MIGHT BE BECAUSE OF EVAPORATION

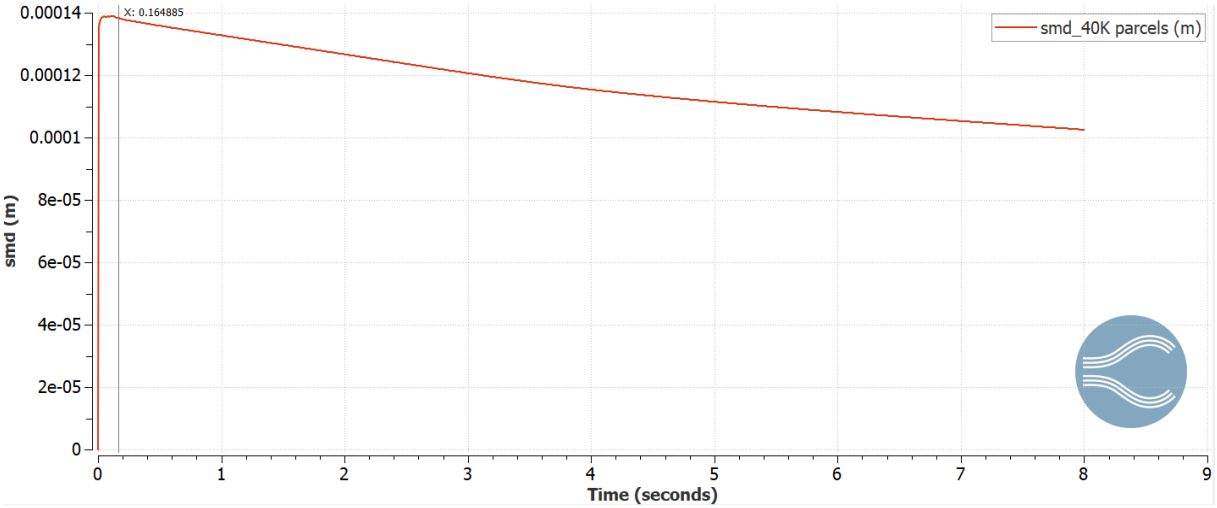

FIGURE 47 SMD 40 000 PARCELS

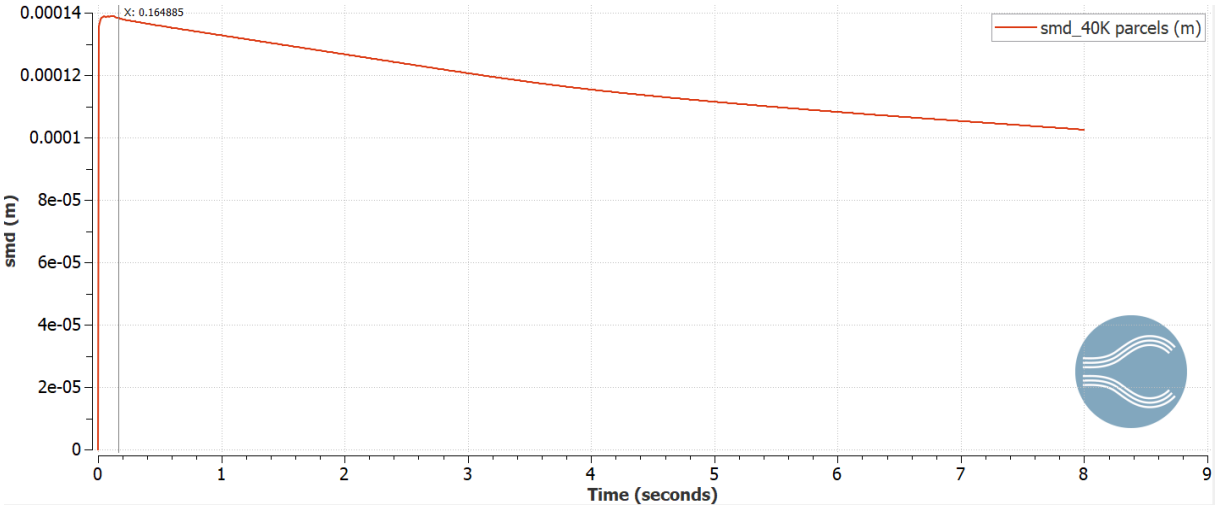

FIGURE 48 SMD 20 000 PARCELS

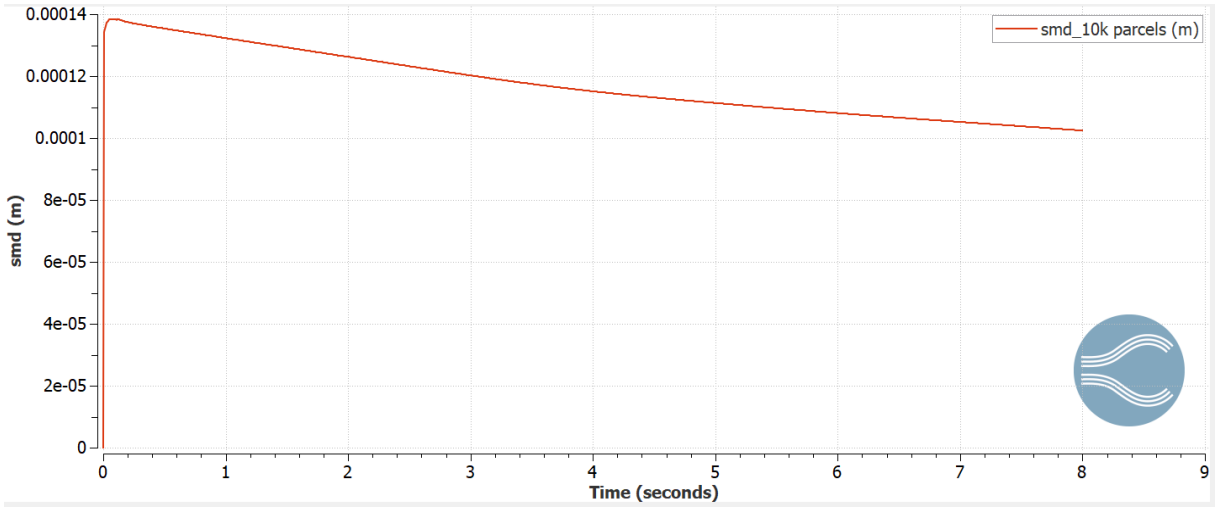

FIGURE 49 SMD 10 000 PARCELS